

國立交通大學
光電工程研究所

碩士論文

五苯環有機薄膜電晶體的氨氣感測器研究

Development of Highly Sensitive Ammonia Gas
Sensor using Pentacene-Based Organic Thin
Film Transistors

The logo of National Tsing Hua University is a circular seal. It features a central emblem with a book and a torch, surrounded by the university's name in Chinese and English. The year '1896' is inscribed at the bottom of the seal.

研究生：吳玉玫

指導教授：冉曉雯 博士

中華民國 九十九年 六月

五苯環有機薄膜電晶體的氨氣感測器研究

**Development of Highly Sensitive Ammonia Gas Sensor using
Pentacene-Based Organic Thin Film Transistors**

研 究 生：吳玉玫

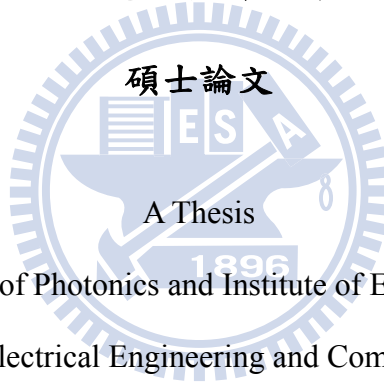
Student: Yu-Mei WU

指 導 教 授：冉曉雯

Advisor: Hsiao-Wen ZAN

國立交通大學

光電工程研究所



Submitted to Department of Photonics and Institute of Electro-Optical Engineering

College of Electrical Engineering and Computer Science

National Chiao Tung University

in partial Fulfillment of the Requirements

for the Degree of

Master

in

Electro-Optical Engineering

June 2010

Hsinchu, Taiwan

中華民國九十九年六月

五苯環有機薄膜電晶體的氨氣感測器研究


研究生：吳玉玫

指導教授：冉曉雯 博士

國立交通大學

光電工程研究所碩士班

摘要



近年來有機薄膜電晶體感測器引起了大量的研究，在醫療的肝病檢測上，非侵入式的氨氣感測器可藉由檢測病人的呼氣氨濃度，取代傳統的血氨濃度檢測。為了能夠將有機薄膜電晶體真正應用到醫療的氨氣檢測上，我們必須將其對氨氣的感測能力提升至 0.5~5 ppm。

透過五苯環有機薄膜電晶體在不同氨氣濃度下的電性量測分析，如電流、臨界電壓、載子遷移率、次臨界電壓等參數，形成多參數的氣體感測器，為了能提升其對氨氣的感測能力，我們透過 UV 光改變其 PMMA 介電層的官能基，使元件對氨氣的反應提升至 0.5 ppm。此外，我們也探討了環境中的水氣分子對元件的影響，以及元件對其他氣體的反應，如氮氣、酒精、二氧化碳、丙酮、甲烷等，建立其對氣體選擇性。綜合以上的研究，我們可以確立五苯環有機薄膜電晶體在氨氣感測的可能性，使其更進一步的應用到醫療檢測上。

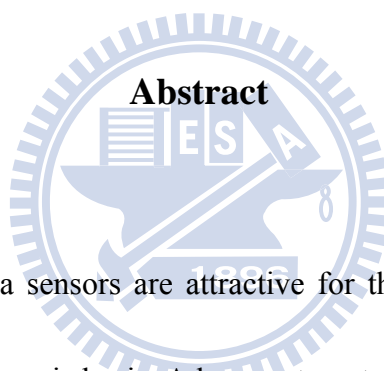
Development of Highly Sensitive Ammonia Gas Sensor using Pentacene-Based Organic Thin Film Transistors

Student: Yu-Mei WU

Advisor: Hsiao-Wen ZAN

Institute of Electro-Optical Engineering

Nation Chiao Tung University, Taiwan



Abstract

Non-invasive ammonia sensors are attractive for the diagnoses of a variety of chronic diseases such as liver cirrhosis. A low cost pentacene-based organic thin film transistor (OTFT) fabricated by a novel and simple process was demonstrated to be highly sensitive and specific for ammonia gas. Measurement parameters of OTFT device characteristics for ammonia detection were investigated. The significant variations of the turn-on current, intrinsic mobility, subthreshold swing and threshold voltage (V_{th}) were observed. The OTFT device detected low concentration (0.5~5 ppm) ammonia gas at room temperature that can distinguish between healthy person and patients with liver cirrhosis and renal failure. The sensitivity of the device was

further enhanced with a simple UV irradiation treatment to modify the functional-end groups of poly(methyl methacrylate) (PMMA) dielectric layer. Possible interferences for ammonia detection such as humidity effect, recovery phenomenon, and sensing selectivity among nitrogen, alcohol, carbon dioxide, acetone, methane and ammonia were also discussed. We concluded that the proposed pentacene-based OTFT is a promising device for the future application in non-invasive medical diagnoses.



致謝

時光飛逝，轉眼間我就要碩士畢業了，回首碩士班的日子，最感謝的是我的指導教授-冉曉雯老師帶領我進入半導體物理的知識殿堂，實驗的過程中進一步地教導我研究的態度，不但培養了我解決問題的能力，也激發了我的潛能，此外，也謝謝老師願意給我機會、鼓勵我去法國攻讀雙聯學位，使我更能獨當一面，能更勇敢的迎向未知的挑戰。

我也非常的謝謝實驗室的大家，謝謝國錫、士欽、周董、武衛、蔚宗學長們在我有問題時都能像你們請教；謝謝文馨、芸嘉、顏志宇、方哥、吳權陵學長姐們教導我機台操作；更感謝淑玲、小寶、繁琦、歐陽你們陪我度過苦悶的研究生生活，有你們一起熬夜作 run 再晚也不會累，即使低潮也能一起互相加油打氣；還有 michael、小能、達欣、威豪、王建敏、小哈、羅世益、長紘、小辛，和你們聊天總是很開心；也很謝謝伍佰幫我喚回記憶、蠶北鼻讓我沒有成為孤單老人、古明哲口試前的玩具直升機；還有 AOSO 實驗室的大家：真的很強的強哥、大帥哥恩禎、燈一直被打開的撒撒、做事認真的楊哥、可愛的葉翰政和葉寶貝、同鄉的 shut down 哥、老實的林洪正、總是很嗨的戴銘志學長、榮總的小白鼠們，謝謝你們讓我在交大的最後三個月有著快樂的回憶。

此外，也非常感謝一起合作的楊裕雄教授實驗室，謝謝楊老師提供設備以及對於研究方向的指導，也謝謝羅淵仁學長還有榮總醫院的協助。

最後，謝謝我寶貝父母親對我的栽培和疼愛，也謝謝我男朋友對我的鼓勵與包容。

CONTENTS

Chinese Abstract	i
English Abstract	ii
Acknowledgment	iv
Contents	v
Figure Captions	vii
Table Captions	ix
Chapter 1: Introduction	1
1.1 Introduction of Organic Thin Film Transistors (OTFTs)	1
1.1.1 Overview of Pentacene-Based Thin Film Transistors	1
1.1.2 Device Structure	2
1.1.3 Organic Semiconductor Material	2
1.1.4 Operating mechanisms of OTFTs	3
1.2 Ammonia Sensor and Their Applications	4
1.2.1 Application of Ammonia Sensors	4
1.2.2 Different Types of Ammonia Sensors	5
1.3 OTFTs Ammonia Gas Sensors	7
1.4 Motivation	8
Figure	10
Chapter 2: Experiment Setup	13
2.1 Fabrication of Organic Thin-Film Transistors	13
2.2 Gas Sensing System	15

2.3 Parameter Extraction	16
2.3.1 Field Effect Mobility	16
2.3.2 Threshold voltage	17
2.3.3 Subthreshold swing	18
Figure	19
Chapter 3: Results and Discussion	20
3.1 Ammonia-sensing phenomenon of standard OTFTs	20
3.1.1 Electrical Properties of Standard OTFTs	20
3.1.2 Gas Diffusion Model	20
3.1.3 Ammonia Concentration Effect	22
3.2 Ammonia-sensing Phenomenon of UV-treated PMMA OTFTs	23
3.2.1 Electrical Properties of UV-treated PMMA OTFTs	23
3.2.2 Sensing phenomenon of UV-treated PMMA OTFTs	25
3.3 Selectivity of Gas Sensing	26
3.4 Phenomenon of Recovery	27
3.5 Influences of Environment Humidity	28
Figure	31
Chapter 4: Conclusion	44
References	45

Figure Captions

Figure 1-1. (a) Top contact and (b) Bottom contact structure

Figure 1-2. Pentacene molecular structure

Figure 1-3. Energy scheme of the gold-pentacene interface

Figure 2-1. Structure of OTFTs

Figure 2-2. Photo images of sensing system

Figure 3-1. Transfer characteristics of standard OTFTs

Figure 3-2. I-V curve of standard OTFTs under 1ppm NH₃ with different time

Figure 3-3. The parameters variation of OTFTs under 1 ppm NH₃ with different time

Figure 3-4. Illustration of scattering effect and traps for gas sensing

Figure 3-5. Illustration of screen effect for gas sensing

Figure 3-6. Energy band of (a) standard OTFTs and (b) Ammonia sensing PMMA

OTFTs

Figure 3-7. (a) Threshold voltage shift and (b) mobility variation versus different

ammonia concentration measured in 1000 seconds and 2000 seconds

Figure 3-8. Simulation of PMMA and UV-treated PMMA estimated by Gaussian 03

with *ab initio* calculation.

Figure 3-9. Transfer characteristics of UV-treated PMMA OTFTs

Figure 3-10. Energy band of (a) standard OTFTs and (b) UV-treated PMMA OTFTs

Figure 3-11. AFM images of pentacene film deposited on (a) PMMA and (b)

UV-treated PMMA

Figure 3-12. (a) Threshold voltage shift (ΔV_{th}) (b) mobility variation (μ/μ_0) and (c)

drain current variation (I/I_0) versus ammonia concentration in different waiting time

of standard OTFTs and UV-treated PMMA OTFTs

Figure 3-13. Threshold voltage shift (ΔV_{th}) and mobility variation ($(\mu_0-\mu)/\mu_0$)

percentage for standard and UV-treated OTFTs when devices were exposed to

different kinds of gas molecules.

Figure 3-14. Mobility variation versus different time of (a) standard OTFTs and (b)

UV-treated PMMA OTFTs under different ammonia concentration from 0 second to

3000 seconds

Figure 3-15. Threshold voltage shift versus different time of (a) standard OTFTs and

(b) UV-treated PMMA OTFTs under different ammonia concentration

Figure 3-16. Threshold voltage shift versus different NH_3 concentrations in the dry

ambient (RH=0%) and in the wet ambient (RH=50%) of (a) standard OTFTs and (b)

UV-treated PMMA OTFTs

Figure 3-17. (a) Mobility variation and (b) drain current variation versus different

NH_3 concentrations in the dry ambient (RH=0%) and in the wet ambient (RH=50%)

of standard OTFTs or UV-treated PMMA OTFTs

Table Captions

Table 1. Diseases associated with unusual breath odors

Table 2. Gas concentration with different healthy condition



Chapter 1

Introduction

1.1 Introduction of Organic Thin Film Transistors (OTFTs)

1.1.1 An Overview of Pentacene-Based Thin Film Transistors

Organic thin film transistors (OTFTs) based on conjugated polymers, oligomers, or other molecules have received much attention for more than a decade. Efforts have also been made to understand the material properties and device physics [1,2,3,4]. Compared to amorphous silicon device, OTFTs have advantages for the low cost, flexibility, low-temperature, and large area processing, etc. Despite the extensive research efforts to discover better materials for the active layer of OTFTs, pentacene is one of the most widely used small molecules for device applications due to its high field effect mobility and easy film formation properties [1,5,6,7]. Recently, pentacene-based thin-film transistors (TFTs) are developed for sensors, display backplane and radio frequency identification devices [8,9,10]. Nevertheless, there are still several issues to be considered before realizing the applications of pentacene TFTs: threshold voltage hysteresis, gate voltage stress resistance and the environment- or ultraviolet (UV) - induced degradation of the pentacene channel [11,12,13,14]. It needs more effort to research and improve these uncertain issues.

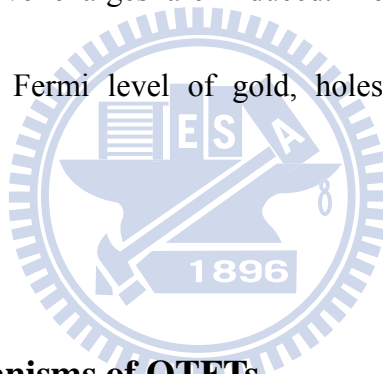
1.1.2 Device Structures

In general, OTFTs are made of three parts: an insulator, a thin film of organic semiconducting material, and three electrodes. Two of the electrodes, the source and the drain, are in direct contact with the semiconductor to apply a source-drain voltage and measure the source-drain current that flows through the organic thin film. The third electrode, the gate, is isolated from the semiconductor by the insulator to modulate the magnitude of the source-drain current. Because most organic semiconductors are fragile materials, the deposition of organic semiconductors on the insulator is much easier than the converse. Thus, the majority of OTFTs are built with the bottom-gate architecture, which is divided into two structures: top contact and bottom contact, in Fig1-1. In the bottom contact structure, contacts are deposited on the insulator. Thus, the contact resistance in bottom contact is higher than in top contact.

1.1.3 Organic Semiconductor Material

Organic semiconductors are traditionally classified as polymers or small molecules. In our study, we chose pentacene as the organic semiconductor material. Pentacene is based on small molecules which are made up of five benzene rings as

show in Fig1-2. It is the p-type material, because holes are easily to transport than electrons. The principle can be illustrated with Fig1-3, the energy scheme of the gold-pentacene interface [15]. HOMO presents highest occupied molecular orbital, and LUMO presents lowest unoccupied molecular orbital. When a positive voltage is applied to the gate, negative charges are induced in the source. However, the LUMO level of pentacene is quite far from the Fermi level of gold. It is very hard for the electrons to inject into the pentacene film. In contrast, when a negative voltage is applied to the gate, positive charges are induced. Because the HOMO level of pentacene is close to the Fermi level of gold, holes can easily inject into the pentacene.



1.1.4 Operation mechanisms of OTFTs

The operation mechanisms of OTFTs are originated from MOSFET. Both OTFTs and MOSFET have semiconductor layer, insulator layer, and three electrodes. But traditional MOSFET are operated in the inversion mode, while the OTFTs are operated in the accumulation mode. Since pentacene is a p-type semiconductor material, holes are the major transport carriers than electrons. When a negative gate voltage is applied, the energy band of the pentacene film bends upwards and causes holes accumulate in the interface between pentacene film and dielectric. It operates

like a capacitor. Because the conductance of the channel is proportional to the charge, it is also proportional to the gate voltage. If we apply a source-drain voltage, the accumulated holes transport from source to drain and result in the source-drain current.

The operation current of OTFTs can be divided into two regions: linear region and saturation region. At low source-drain voltage, the current is proportional to both the gate and drain voltages. When the drain voltage increases to approach the gate voltage, there is a pinch off of the channel, and the channel current becomes independent of the drain bias. So, we call it the saturation region.

1.2 Ammonia Sensor and Their Applications

1.2.1 Application of Ammonia Sensors

Ammonia is an importance compound for living system. It can be widely utilized in many fields, such as chemical industries, fertilizer factories, refrigeration systems, food processing, fire power plants, and medical diagnosis, etc. For applications above, the concentration control of ammonia is very important. For example, in chemical industries, ammonia concentration is related to the quality of fertilizers and frozen foods. Additionally, ammonia concentration plays a role in medical diagnosis. **Tab1** is the component of human breath volatile organic compounds (VOCs) related to some

diseases. It shows that ammonia is a disease marker for the uremia, liver cirrhosis, and renal failure. **Tab2** is the gas concentration with different healthy condition. The ammonia concentration is 1~5 ppm for renal failure and 0.5~1 ppm for liver cirrhosis. The most common method we use for diagnosis is by examining the ammonia concentration of the blood. Recently, developments of a non-invasive diagnostic method have received considerable attention. If we can develop a non-invasive, inexpensive, portable and disposable diagnostic device, patient's breath can be easily detect and traced by the gas sensor.

1.2.2 Different Types of Ammonia Sensors

(a) Metal-oxide gas sensors

Some well-known materials for ammonia gas sensing are ZnO [16], iridium oxide [17], molybdenum oxide [18], polyaniline [19,20,21], polypyrrole [22], Au and MoO₃-modified WO₃ [23,24], Pt- and SiO₂-doped SnO₂ [25], etc. When the device is exposed to analytes, the gas removes some of the adsorbed oxygen and modulates the height of the potential barriers, thus changing the conductivity and creating the sensor signal. However, various ammonia sensors reported work at high temperature such as 350°C, but it is not convenient to sense at such high temperature. Despite of high sensibility (from 1 to 1000 ppm), selectivity and stability, the application of these

sensors remains limited.

(b) Catalytic ammonia sensors

Catalytic ammonia sensor is based on the catalytic reaction of a metal layer with ammonia gas. The reaction will cause a change in electrode potential and the charge carrier concentration which can be quantified by using a field effect device, like a capacitor or a transistor [26,27]. The detection limit can be 1 ppm.

(c) Conducting polymer gas detectors

Conducting polymer ammonia gas detectors use polymer, like polypyrrole and polyaniline, to react with ammonia. During the process, ammonia can reversibly reduce the oxidized form of polymer. Because the reduction of the polymer film causes a change in the conductivity of material, we can use it to make resistometric or amperometric ammonia detection [28,29]. However, the irreversible reaction between ammonia and the polymer causes the sensitivity of the sensor decrease when exposed to ammonia. The detection limit is about 1 ppm.

(d) Optical gas analyzers

There are two optical methods for the detection of ammonia. One is Berthelot reaction,

which uses coloration reaction of ammonia with phenol and hypochlorite in aqueous solutions [30,31]. One drawback is the slow kinetics of the reaction. The detection limit is about 5 μM of ammonia in water or 90 ppb. The second method is optical absorption ammonia detection [32]. By using a laser and a spectrograph, we can get a spectrum of the light influenced by the gas composition. Although the method is very sensitive and selective for ammonia sensing, the equipment is very expensive and it is not suitable for miniaturized ammonia sensors.

1.3 OTFTs Ammonia Gas Sensors

The research of OTFT sensors started in the late 1980s, just after the first OTFTs was proposed. Such sensors offer the advantages of simple process, low fabrication cost, remarkable response repeatability [33] and selectivity [34,35]. Because many types of organic molecules exhibit sensing behavior based on their chemical compositions, sensibility and selectivity can be pursued by choosing ad hoc chemically or biologically functionalized semiconducting polymer active layers for the use of OTFTs in compact sensing systems or in bio-chips [33,36,37,38]. In addition, [36,39] provided evidences that the OFET sensor has better performance than a similar resistor-type sensor in drift, sensitivity, signal-to-noise ratio, response time, lifetime, and operating temperature. Particularly, OTFTs have been proposed as

multi-parameter sensors [40]. By measuring the parameters of field-induced conductivity, threshold voltage, and field-effect mobility, we can get a fingerprint of each gas. It makes the transistors to be more selective than conventional chemiresistors. Besides, the morphology of active layer plays an important role on the sensibility of OTFT sensors. The device response increases when the grain size is reduced [41]. The effect of a channel length comparable to the grains size has also been observed. In order to lower the limit of detection, nanoscale organic transistors have been explored [42].

So far, the active layer of OTFT sensors include substituted thiophene polymers, oligomers, naphthalenes, copper-phthalocyanine, pentacene and others. These devices were exposed to different analytes, such as alcohols, ketones, thiols, nitriles, ester and ring compounds. However, it does not have much research of ammonia sensors with OTFTs. Our studies of pentacene-based OTFTs applied on ammonia sensor were the first.

1.4 Motivation

In order to develop a non-invasive, inexpensive, portable and disposable diagnostic device, we use pentacene-based OTFT to act as ammonia sensor. It is very important to find out the sensing mechanism and summarize the variation of

parameters in different ammonia concentrations. Furthermore, to enhance the response to ammonia gas, we try to modify the sensing surface to obtain different functional groups which has strong interaction with ammonia gas. Besides, we need to discuss the recovery phenomenon to know whether it can be reverse or not. The humidity of measurement environment will also be considered.



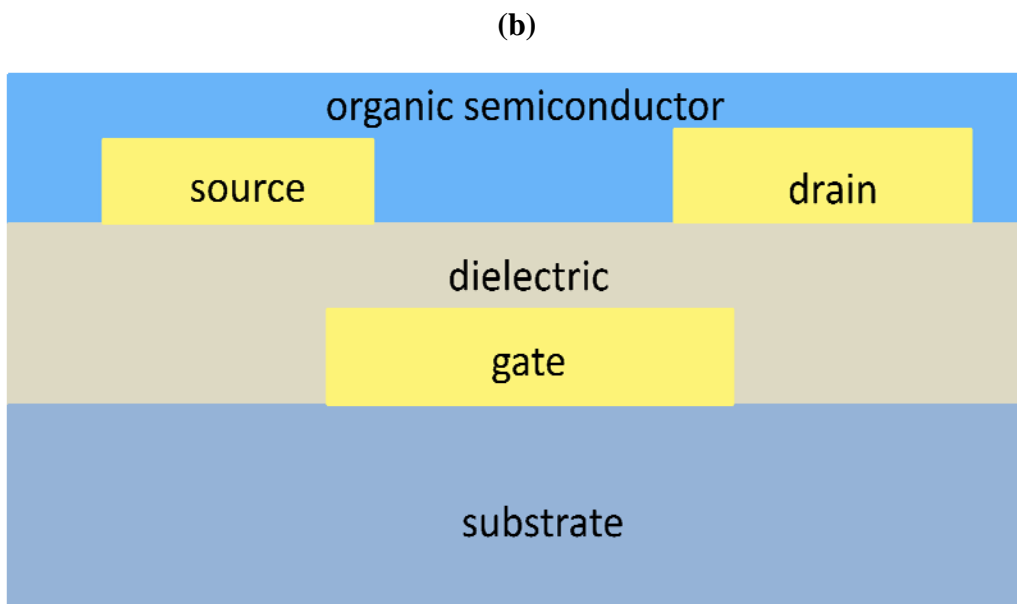
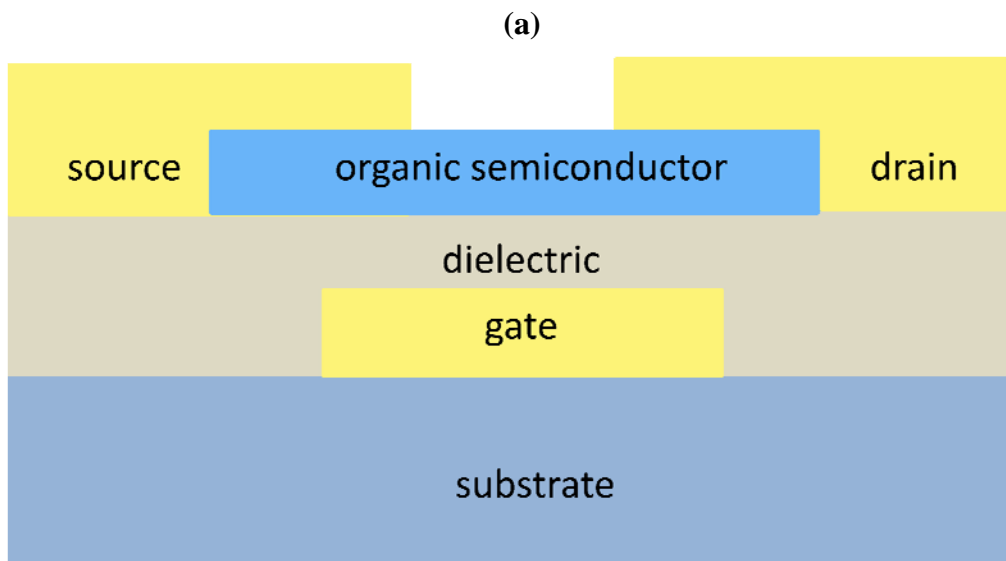
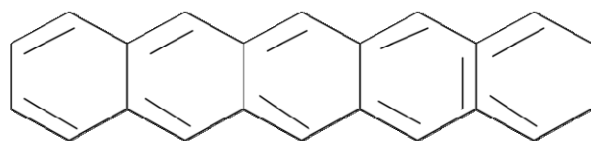


Figure 1-1. (a) Top contact and (b) bottom contact structure



Pentacene ($C_{22}H_{14}$) molecule

Figure 1-2. Pentacene molecular structure

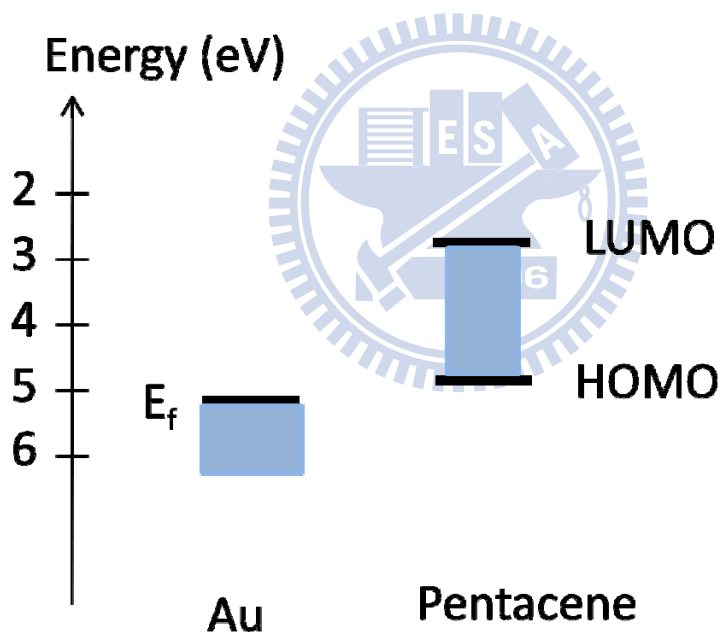


Figure 1-3. Energy scheme of the gold-pentacene interface

Breath component as a disease marker	Diseases	References
Acetone	Diabetes; lung cancer	Ebeler et al., 1997 Grote et al., 1997
Ammonia	Uremia; Liver Cirrhosis Renal failure	Manolis, 1983 Davies et al., 1997
Butyric acid	Liver Cirrhosis	Manolis, 1983
Ethanol	Liver Cirrhosis	Manolis, 1983
Hydrogen sulfide	Periodontal disease	Manolis, 1983
Carbon dioxide	H. Pylori infection	William, 2007

Table 1. Diseases associated with unusual breath odors

Disease Gas	Renal failure	Liver Cirrhosis	Diabetes	References
	Ammonia	4.8 ppm	0.5~1 ppm	
Acetone			5-300 ppm	Zhang, 1970

Table 2. Gas concentration with different healthy condition

Chapter 2

Experiment Setup

2.1 Fabrication of Organic Thin-Film Transistors

We chose highly-doped p-type silicon wafers with 100 nm thick silicon oxide as the substrate. The p-type silicon was used as gate electrode, and the silicon oxide layer was used as gate insulator. After cleaned with 5min de-ionized water-5min acetone-5min de-ionized water, the particles and the impurities on the substrate were removed in order to avoid gate leakage which may cause instability [43].

Then, soluble poly(methyl methacrylate) (PMMA) was spun on the silicon oxide layer by the spin coater to improve the electric performance and increase the grain boundaries [44]. The PMMA was obtained from MicroChem. Corp. with a molecular weight of 95000 and was dissolved in anisole at 10 wt %. The spin speed was accelerated from 0 to 1000 rpm during the first 10 seconds and further increased to 7500 rpm during the following 10 seconds. After kept as 7500 rpm for 40 seconds, the spin speed was decreased from 7500 to 1000 in the following 10 seconds and further decreased to 0 rpm during 10 seconds. After the process of spin coating, the PMMA layer was annealed by hot plate with 90°C for 30 minutes. The capacity of PMMA/SiO₂ dielectric layer was about 23~24 nF/cm². Besides, some of the samples

were then exposed to UV-light, whose wavelength is 175~285 nm and the output power is 40 mW, for 60 seconds to change the functional group of PMMA.

Following, the pentacene material obtained from Aldrich with 99.9% purity was evaporated through a shadow mask on the UV treated and non-UV treated PMMA/SiO₂ dielectric layer as the active layer. The deposition was started at the pressure around 3×10^{-6} torr and the temperature was kept at 20°C. The deposition rate of 1000-Å-thick pentacene was 0.1 Å/sec at the first 100Å and was smoothly increased to 0.5 Å/sec at the 200Å to the 1000Å. The deposition temperature, the deposition pressure and the deposition rate are the important parameters to decide the ordering quality of the organic film [45].

Finally, we used gold as the source and drain electrodes. Due to its similar work function with pentacene, we can get better injection from gold to pentacene film. Before gold deposition, we deposited 50-Å-thick nickel through a shadow mask on the pentacene film as the adhesion layer. Then, we deposited 1000- Å-thick gold on the samples. The width (W) and length (L) of the device's channel were 800 μm and 1200 μm, respectively. The geometry of the OTFTs is shown in Fig2-1.

2.2 Gas Sensing System

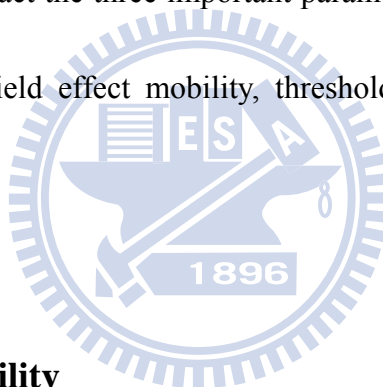
In this study, we used OTFTs devices to sense five different kinds of gas as following: ammonia (NH_3), methane (CH_4), acetone (CH_3COCH_3), alcohol ($\text{C}_2\text{H}_5\text{OH}$) and carbon dioxide (CO_2). To control the environment in the precise condition, we measured the devices with a semiconductor analyzer (Keithley 4200-SCS) in a sealed chamber. The inside volume of the chamber is about 42 L and its configuration image is shown in Fig2-2. After putting the device into the chamber, we vacuumed it to the pressure of 10^{-1} torr and then purged it with high purity nitrogen (99.99% N_2) to the pressure of 1 atm. This process can avoid the influence of moisture and other gases we did not want to sense. Thus, the data measured in the N_2 ambience was the standard data. Then, we injected the gas we wanted into the chamber and measured the device's characteristic.

The concentration of NH_3 was controlled as 0.5, 1, 3 and 5 ppm (mg/L) by a mass flow controller (MFC). CH_4 and CO_2 gases were also injected through a MFC and their concentrations were controlled as 2 ppm. To get CH_3COCH_3 and $\text{C}_2\text{H}_5\text{OH}$ gases, we used a Tedlar bag and put liquid CH_3COCH_3 and $\text{C}_2\text{H}_5\text{OH}$ inside. After liquid CH_3COCH_3 and $\text{C}_2\text{H}_5\text{OH}$ evaporated to saturate pressure, we injected the gases into the chamber with a syringe which can control the concentration as more than 2 ppm.

To discuss the influence of moisture during the gas sensing process, we also provided different relative humidity (RH) environment. By using a N₂ flow to pump water, water vapor can be introduced into the chamber. We controlled the RH value as 0% and 50% with different input time and measured the RH with a hygrometer.

2.3 Parameter Extraction

It is also important to analyze the data with a good method. In this section, I introduce the method we used to extract the three important parameters of the devices from the electrical characteristics: field effect mobility, threshold voltage, and subthreshold swing.



2.3.1 Field Effect Mobility

Field effect mobility is an important parameter because it is directly related to the orientation of the active layer. When other molecular transports into the bulk of the active layer, the orientation of the active layer will be influenced and the field effect mobility will also be changed. Because the characteristics of pentacene-based thin film transistors are similar to conventional MOSFETs, we used the same method to extract mobility from the transconductance maximum g_m in the linear region:

$$g_m = \left[\frac{\partial I_D}{\partial V_G} \right]_{V_D = \text{constant}} = \frac{WC_{ox}}{L} \mu V_D$$

$$\mu = \frac{g_m}{\left(\frac{W}{L} C_{ox} V_D \right)}$$

, where W is the width, L is the length of the channel, and Cox is the capacitance of the dielectric layer.

2.3.2 Threshold Voltage

Threshold voltage is also an important parameter because it strongly depends on dielectric surface states. When the device was exposed to a gas, which might create charge sites on the dielectric surface, the threshold voltage shifted. With the drain current in the linear region:

$$I_D = \frac{W\mu C_{ox}}{L} \left[(V_G - V_T)V_D - \frac{V_D^2}{2} \right]$$

which can be simplified for $V_D \ll (V_G - V_T)$ to

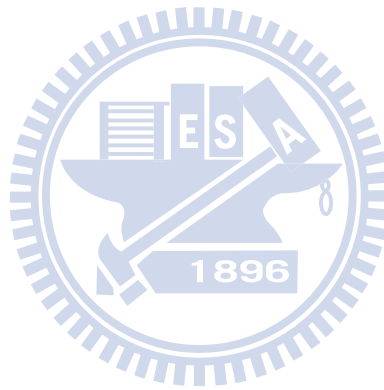
$$I_D \cong \frac{W\mu C_{ox}}{L} [(V_G - V_T)V_D] \quad (1)$$

, we extracted the threshold voltage by finding out the intersection point of the drain current versus gate voltage in the linear region.

2.3.3 Subthreshold Swing

Subthreshold swing represents how rapidly the device turn on from the off state. It is related to the interface quality and the defect density of the device. We extract subthreshold swing with

$$S = \left. \frac{\partial V_G}{\partial(\log I_D)} \right|_{V_D = \text{constant}}$$



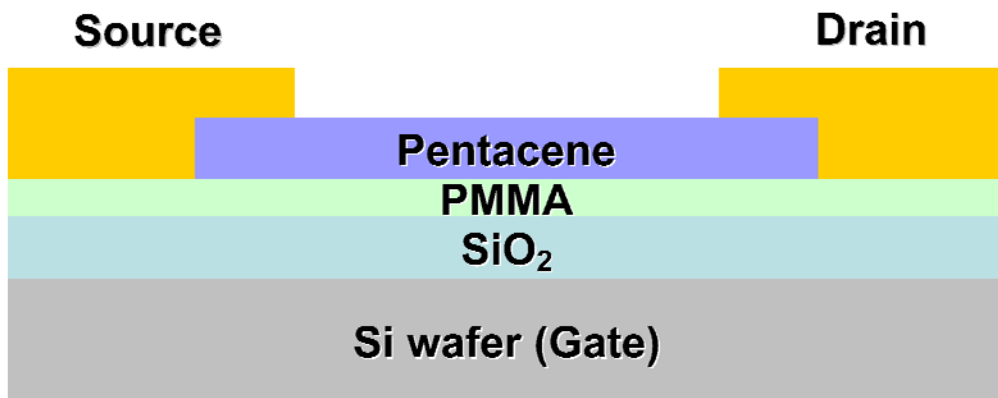


Figure 2-1. Structure of OTFTs

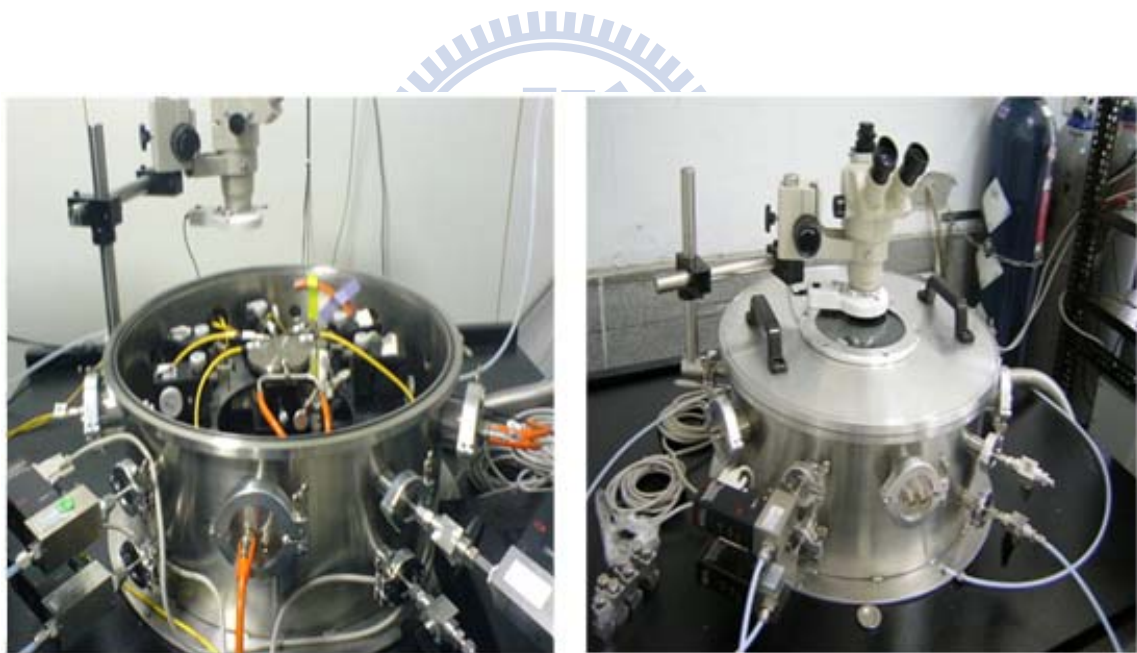


Figure 2-2. Photo images of sensing system

Chapter 3

Result and Discussion

In this chapter, we first discussed the gas-sensing phenomenon of standard OTFTs. Then, we introduced the UV-treated PMMA method to improve the sensitivity of OTFTs. Besides, we also discussed the selectivity and the phenomenon of recovery. Finally, we increased the relative humidity to find out the environment influence of the water.

3.1 Ammonia-sensing Phenomenon of Standard OTFTs

3.1.1 Electrical Properties of Standard OTFTs

Before exposing the device on the analytic gas, we measured the electrical characteristics of the device at constant drain bias, $V_d = -3$ V, and sweeping gate bias from 5 V to -40 V. With the Fig3-1, we can extract the threshold voltage as -16.4 V, the mobility as $0.3 \text{ cm}^2/\text{Vs}$, and subthreshold swing as 0.66 V/decade. Those data was taken as standard one to be compared with other data under gas-sensing.

3.1.2 Gas Diffusion Model

Fig3-2 presents the I-V curve under 1 ppm NH_3 condition with different time. As

shown in Fig3-3, the variations of the turn-on current, field-effect mobility, and threshold voltage shift were decreased while the subthreshold swing was increased. The turn-on current variation (I_d/I_{d0}), according to Eq(1), is affected by both threshold voltage shift (ΔV_{th}) and mobility variation (μ/μ_0), where I_{d0} and μ_0 are the initial drain current and the initial field-effect mobility.

The reason for the decreasing of mobility and threshold voltage is still not very clear. A possible reason is that positive ammonia ions (NH_4^+) or polar ammonia molecular (NH_3) penetrated through the grain boundaries into the bulk of pentacene layer and created scattering centers or traps [47], as Fig3-4. In addition, the polar molecules may decrease the rate of charge transport in organic materials by increasing the energetic disorder through charge-dipole interactions [48]. Because the concentration of ammonia was fixed, the mobility decreased to saturate very soon.

On the other hand, the threshold voltage was decreased gradually. The reason may be the hole-traps, which were attributed to the NH_3 or NH_4^+ near dielectric interface and caused lower concentration of gate-induced mobile carriers [49], as Fig3-5. Therefore, it needs more negative gate voltage to induce holes in the p-channel, as Fig3-6. Because it needed more time for the formation of the hole-traps near the interface between pentacene and dielectric layer, the threshold voltage shift could not as fast as the mobility variation. The increased subthreshold swing

conformed that the density of interface traps between pentacene and dielectric layer were increased [46].

3.1.3 Ammonia Concentration Effect

To confirm the gas sensing model, we exposed the devices to different ammonia concentration from 0.5ppm to 5ppm. Fig3-7 (a)(b) shows the threshold voltage shift and mobility variation versus different ammonia concentration measured in different time (1000 seconds and 2000 seconds). It clearly shows that the threshold voltage shift and mobility variation were increased with the increasing of ammonia concentration, which caused more NH_4^+ or NH_3 penetrate through the grain boundaries of pentacene film. We can also find that after waiting for 2000 seconds, the threshold voltage shift more than waiting for 1000 seconds. However, the mobility variation did not change much between 2000 seconds and 1000 seconds waiting time. The phenomenon conformed to the gas sensing model we mentioned above.

For application to non-invasive diagnostic sensor for cirrhotic patients, it is necessary to monitor ammonia concentration at 0.5 ppm or lower so that the breath samples between healthy person (breath ammonia level: 0.278 ppm) and a patient (breath ammonia level: 0.745 ppm) can be distinguished [50]. For the patients with renal failure, we need to monitor ammonia concentration at 1 ppm (relieve) to 5 ppm

(dangerous) [51]. However, it was hard to distinguish the variation difference between 0.5 ppm and 1 ppm ammonia with the standard OTFTs. Thus, we needed to find another way to improve the sensing ability.

3.2 Ammonia-sensing Phenomenon of UV-treated PMMA OTFTs

To enhance the sensitivity, we used a UV-light irradiation on PMMA to modify the dipole moment of the dielectric surface [52]. The PMMA functional end-groups changed from $-\text{COOCH}_3$ to $-\text{COOOH}$, which will result in the negative charge sites near the PMMA surface. Fig3-8 is the simulation of PMMA and UV-treated PMMA which were estimated by Gaussian 03 with *ab initio* calculation. The dipole moment of standard PMMA and UV-treated PMMA were 1.81~1.91 Debye and 2.42~2.5 Debye, respectively.

3.2.1 Electrical Properties of UV-treated PMMA OTFTs

Fig3-9 is the I-V curve of UV-treated device which was measured at constant drain bias, $V_d = -3$ V, and sweeping gate bias from 5 V to -40 V. The threshold voltage we extracted is -11.1 V, mobility is $0.31 \text{ cm}^2/\text{Vs}$, and subthreshold swing is 0.68V/decade. Compared with standard device, UV-treated device was easily to be

turn on and its subthreshold swing was larger. It may due to the change of functional end-groups (from $-\text{CH}_3$ to $-\text{COOOH}$) produced by UV-treatment on PMMA surface, which will result in the negative charged-states near PMMA surface. With the comparing of the energy band of standard OTFTs Fig3-10(a) and UV-treated PMMA OTFTs Fig3-10(b), the negative charge sites, which produced by UV treatment, caused a surface potential change that induced a bending of the HOMO level at the interface and increased the carrier density in the channel [53,54,55,56,57]. Thus, it did not need so much negative gate voltage to induce holes for turn-on. However, the mobility of both devices was the same. It indicated that the structure of the pentacene film was not affected by UV treatment. Fig3-11 (a)(b) are the AFM images of pentacene film deposited on PMMA and UV-treated PMMA, respectively. We can find that the grains and roughness were almost the same.

To verify the hypothesis, we calculated the number of interface states N_{ss} with the equation [59],

$$N_{ss} = \left[\frac{S.S. \cdot \log(e)}{kT/q} - 1 \right] \cdot \frac{C_{total}}{q}$$

where $S.S.$ is the subthreshold swing, e is the Napierian logarithm, k is the Boltzmann's constant, C is the capacity of total device, q is the electric charge and T

is the absolute temperature.

For standard OTFTs (subthreshold swing = 0.64 V/decade), the number of interface states were $1.43 \times 10^{12} \text{ cm}^{-2} \text{ eV}^{-1}$; for UV-treated OTFTs (subthreshold swing = 0.68 V/decade), the number of interface states were $1.53 \times 10^{12} \text{ cm}^{-2} \text{ eV}^{-1}$. It was reasonable to observe that UV-treated device exhibited higher interface state density than that of standard device.

3.2.2 Sensing Phenomenon of UV-treated PMMA OTFT

We measured the UV-treated PMMA devices at the same condition as standard devices. After extracting the parameters from I-V curve, we found that the threshold voltage shifted much, the mobility and drain current also decreased much compared with standard OTFTs. Fig3-12(a)(b)(c) are the threshold voltage shift, mobility variation and drain current versus ammonia concentration in different waiting time of standard OTFTs and UV-treated PMMA OTFTs, respectively. We proposed that UV radiation increased the dipole moment of dielectric surface and attracted ammonia gas molecules to accumulate near the dielectric surface. Also, the negative charge sites which caused by UV treatment enhanced the attraction of positive ammonia ions (NH_4^+) gave stronger electric responses on UV-treated PMMA OTFTs than those of

standard OTFTs. The variation difference between 0.5 ppm and 1 ppm ammonia can be large enough to be distinguished. Therefore, UV treatment can enhance the ammonia sensitivity.

3.3 Selectivity of Gas Sensing

To research and design an ammonia gas sensor, it is very important to confirm the sensing selectivity. Thus, we exposed the devices to five different kinds of gas that may exist in human's breath, including ammonia (1 ppm), methane (2 ppm), acetone (more than 1 ppm), alcohol (more than 1 ppm) and carbon dioxide (1000 ppm). With **Fig3-13**, we can find that at a fixed sensing time (2000 sec), the threshold voltage shift was not distinct with increased time under the condition of methane (CH₄), acetone (CH₃COCH₃), alcohol (C₂H₅OH) and carbon dioxide (CO₂). Although the concentration of ammonia was the lowest, the threshold voltage shift was evident after 1000 seconds. The variation of mobility under ammonia environment was also the biggest. With the sensing index, threshold voltage shift and mobility variation, we can confirm that both standard and UV-treated OTFTs exhibited good selectivity between ammonia and other gases.

3.4 Phenomenon of Recovery

In order to verify the sensing mechanism, we discuss the phenomenon of recovery. At 0 second, both the standard and UV-treated devices were exposed to nitrogen. Then, during 0 to 3000 seconds, the devices were exposed to 0 ppm (nitrogen), 1 ppm, 3 ppm, 5ppm ammonia gas individually. After that, during 3000 to 4500 seconds, the ambience was purged with nitrogen.

With Fig3-14 (a)(b), we can find that the mobility of both the standard device and UV-treated PMMA device had recovery. Although the value could not recover to the beginning, the phenomenon were immediately when the ammonia was purged out. The recovery of mobility may due to the decreasing of ammonia which may create scattering centers or traps [47].

However, with Fig3-15 (a)(b), the threshold voltage shift of both devices did not have evident recovery. Although the slope of threshold voltage shift was gradual when the ammonia was purged out, the value could not be increased. The reason may be that the ammonia molecular NH_3 or ammonia ions NH_4^+ had been trapped on the interface of the dielectric and pentacene layer. Thus, the reaction could not be reversed.

3.5 Influences of Environment Humidity

In order to know the influence of humidity to the sensing model, we changed the measure environment by increasing the relative humidity (RH) in the chamber. In the wet nitrogen ambient (RH=50%), comparing with dry nitrogen ambient (RH=0%), we can find that the threshold voltage of standard device had a negative shift, as Fig3-16(a). However, in the same condition, the UV-treated PMMA device had a positive threshold voltage shift, Fig3-16(b). It may due to different functional-end group of dielectric. The polar -COOOH functional-end group of UV-treated PMMA can interact with water molecules and create acceptor-like traps [60]. Because extra holes were induced by trapped electrons, the threshold voltage turned positive [58]. Nevertheless, it is hard for less-polar -COCH₃ functional-end group of standard devices to interact with water molecules. When the polar water molecules diffused into the interface between dielectric and pentacene layer, it may attribute hole-traps near dielectric interface and caused lower concentration of gate-induced mobile carriers. Therefore, it needs more negative gate voltage to induce holes in the p-channel.

With the increasing of ammonia concentration, both the standard device and UV-treated PMMA device had negative threshold voltage shift, especially in the wet ambient (RH=50%). Because the threshold voltage shift of water and ammonia was

opposite for the UV-treated PMMA device, we can confirm that something must happen in the wet ammonia ambient. The chemical reaction between water and ammonia,



, may be enhanced due to the increased H_2O , which resulted in more NH_4^+ and less H_2O . Thus, the threshold voltage shifted much to the negative side in wet ammonia ambient.

From Fig3-17(a), we can find that the mobility variations of both standard devices and UV-treated PMMA device were decreased more in wet ambient than in dry ambient. The reduction of carrier mobility was because polar water molecules residing at grain boundaries interact with carriers [61]. Scattering effect or the field screening effect may be the mechanism to describe interactions between polar water molecules and carriers [62]. Because UV-treated PMMA devices have polar surface which can attract more dipole water, the decreased difference between wet and dry ambient of UV-treated PMMA devices were more than standard devices.

For the UV-treated PMMA devices, since threshold voltage moved to positive value in wet nitrogen ambient, there should be an increase of the drain current variation. However, from Fig3-17(b), the drain current variation of UV-treated device was decreased in wet nitrogen ambient. The reduction of drain current may be mainly

attributed to a reduction of mobility [58]. But, we can see the influence of threshold voltage in the difference of decreased current between wet and dry ambient, the variation of UV-treated PMMA devices were smaller than standard devices.



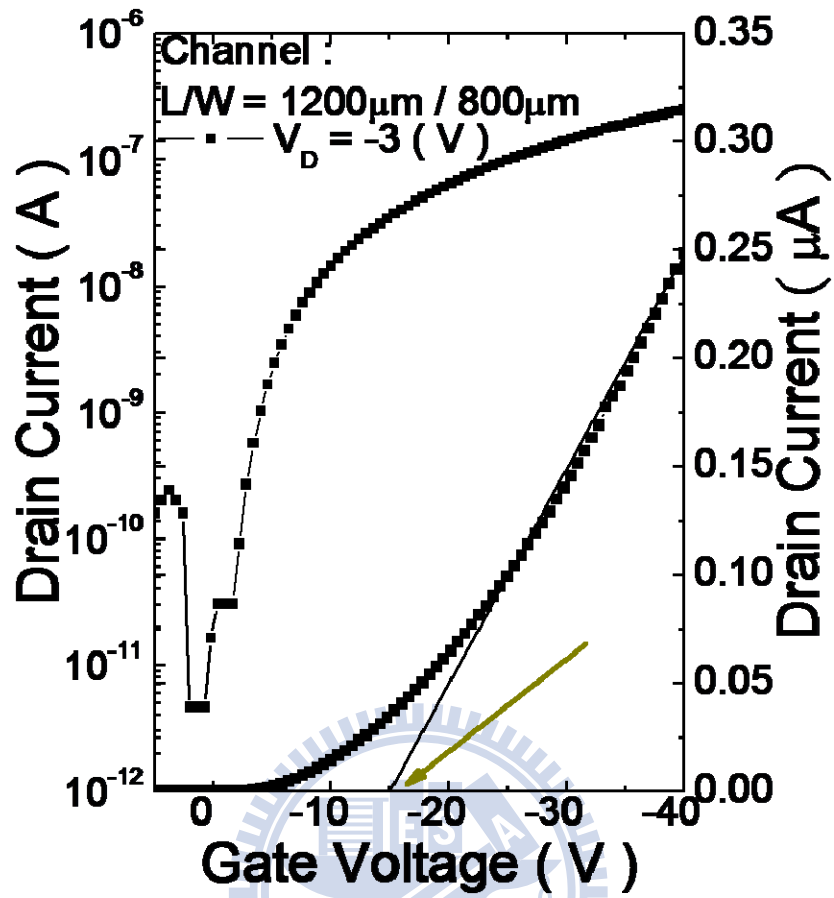


Figure 3-1. Transfer characteristics of standard OTFTs

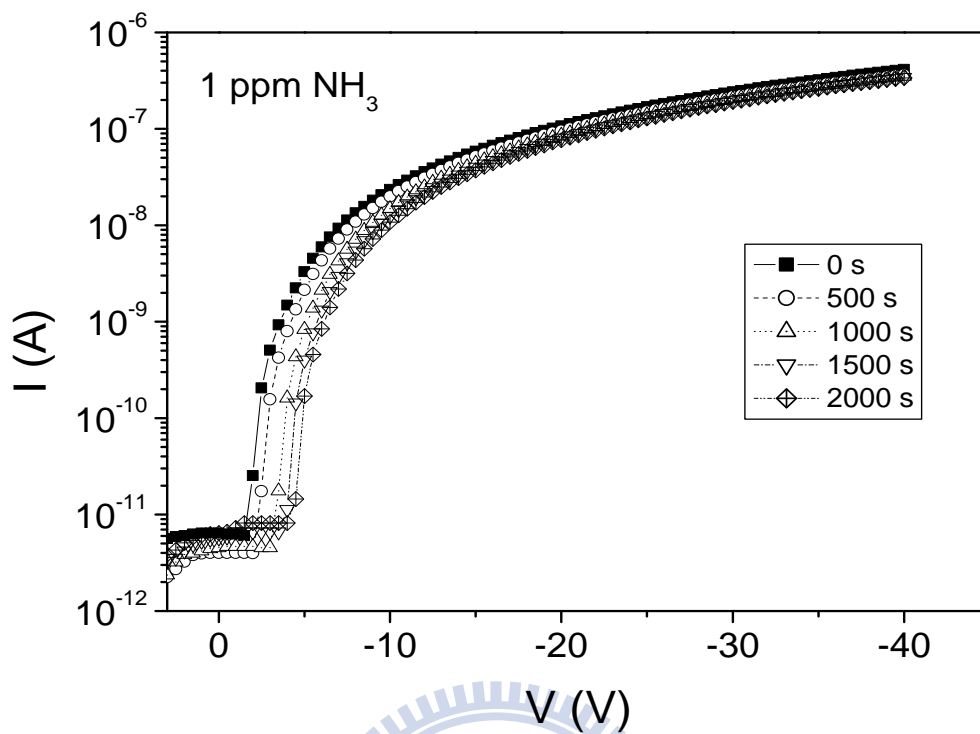


Figure 3-2. I-V curve of standard OTFTs under 1ppm NH₃ with different time

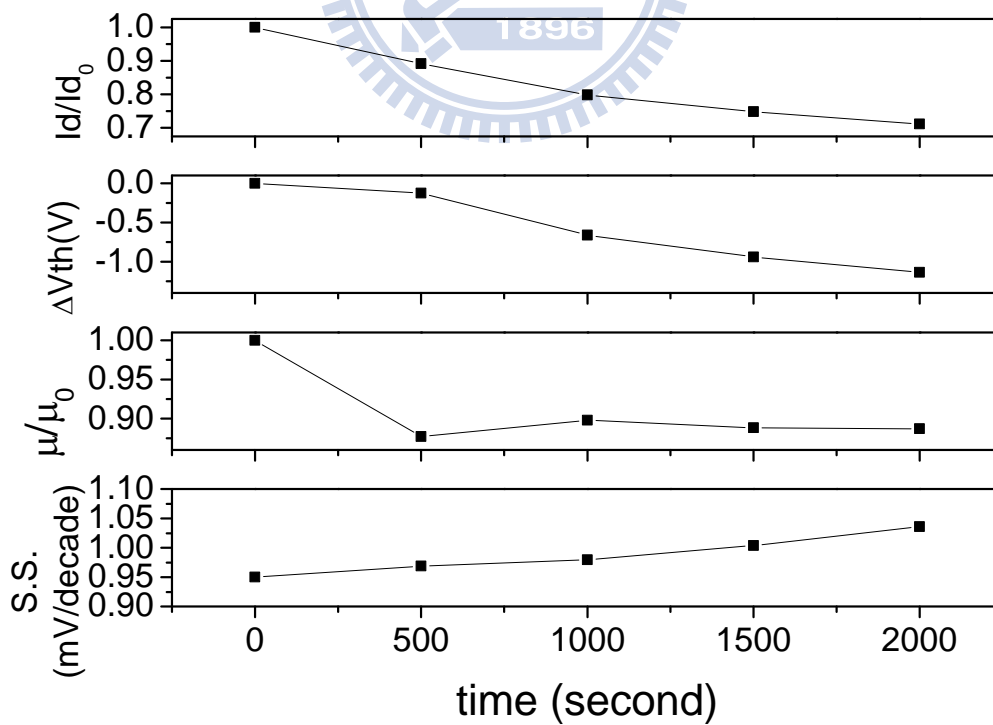


Figure 3-3. The parameters variation of OTFTs under 1 ppm NH₃ with different time

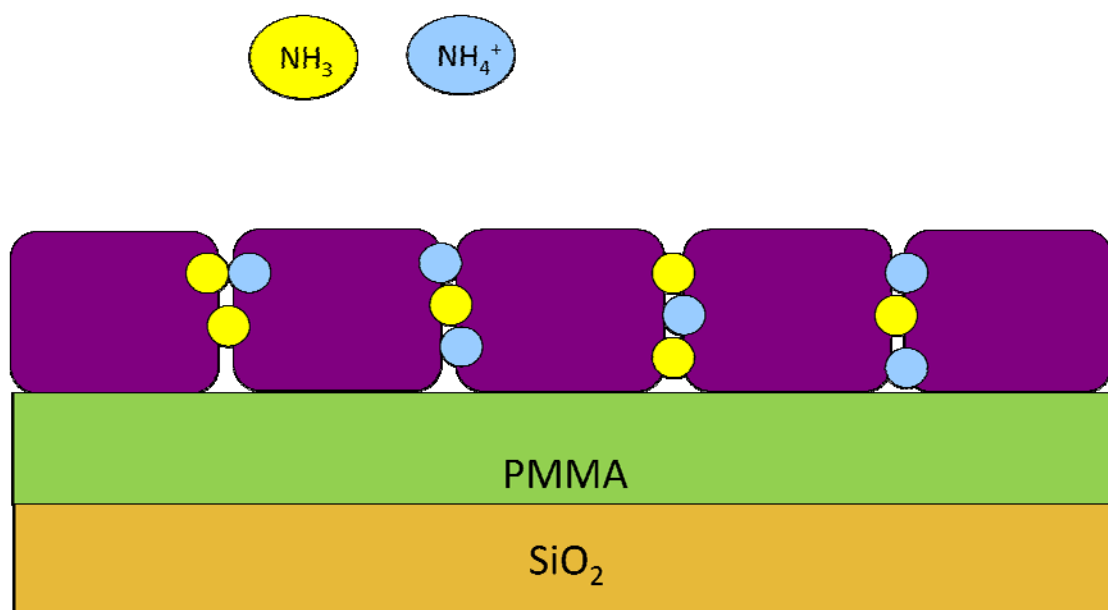


Figure 3-4. Illustration of scattering effect and traps for gas sensing

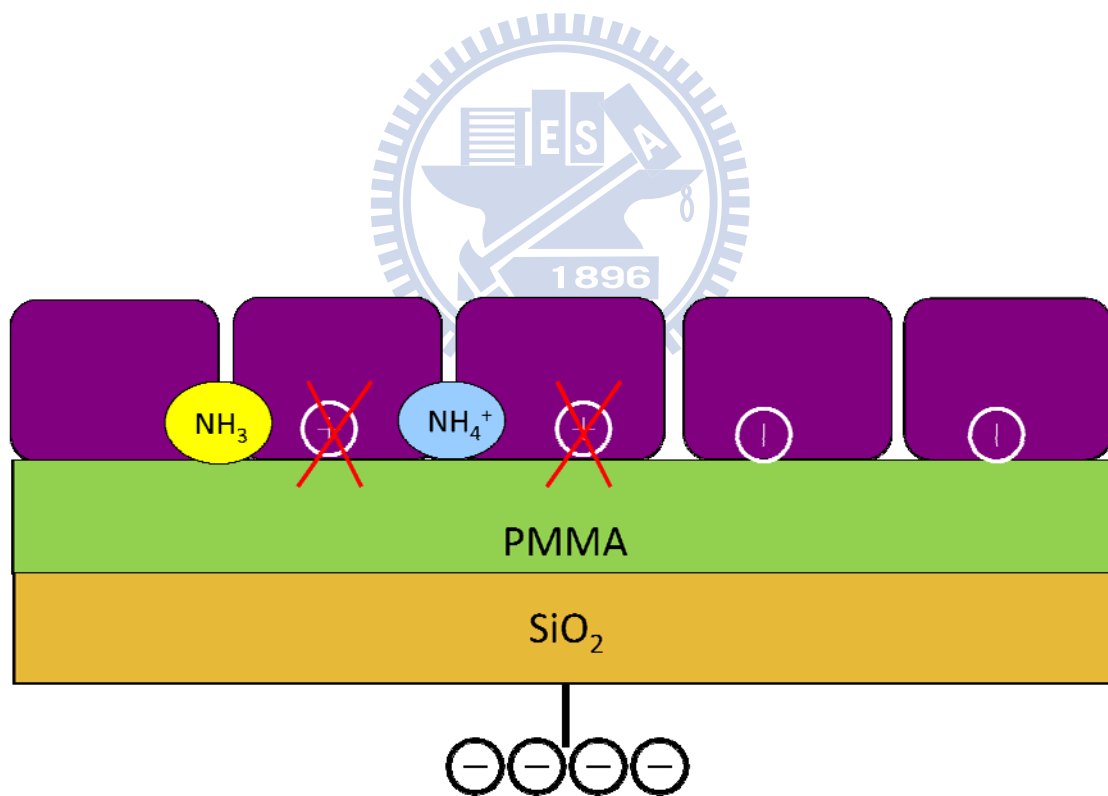


Figure 3-5. Illustration of screen effect for gas sensing

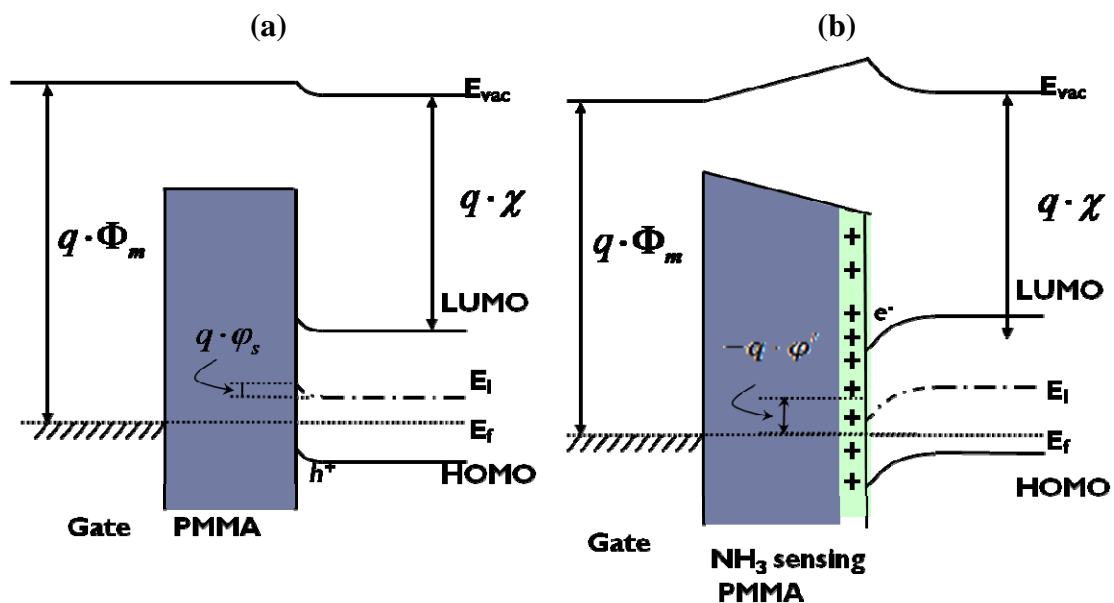


Figure 3-6. Energy band of (a) standard OTFTs and (b) Ammonia sensing PMMA OTFTs

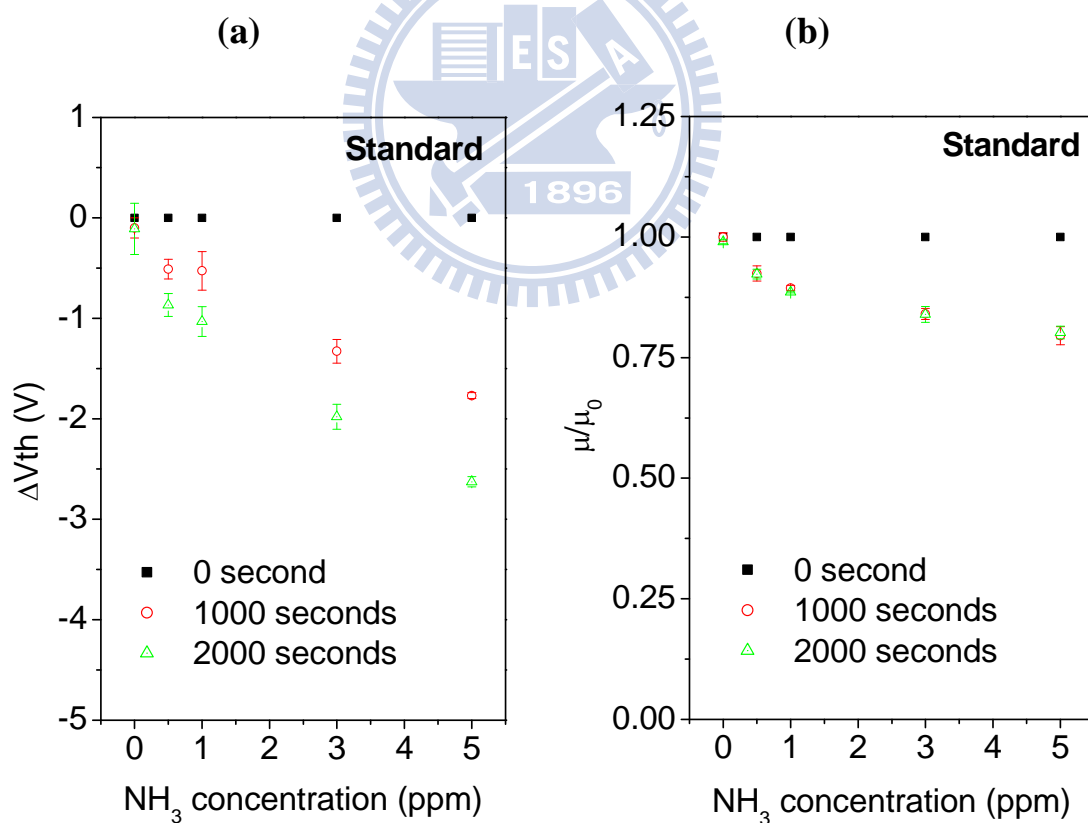
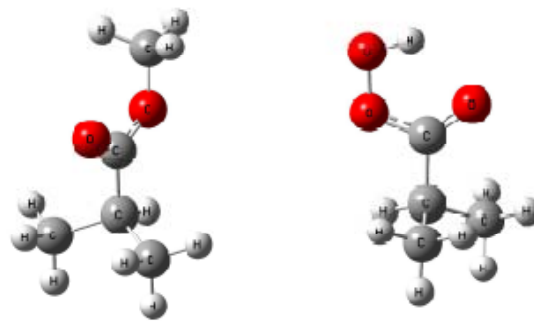


Figure 3-7. (a) Threshold voltage shift and (b) mobility variation versus different ammonia concentration measured in 1000 seconds and 2000 seconds



PMMA UV-treated PMMA

Basis set	Dipole moment (Debye)	
6-311G (d,p)	1.815	2.424
6-311+G (2d,p)	1.894	2.502
6-311+G (2df,2p)	1.912	2.489

Figure 3-8. Simulation of PMMA and UV-treated PMMA estimated by Gaussian 03 with *ab initio* calculation.

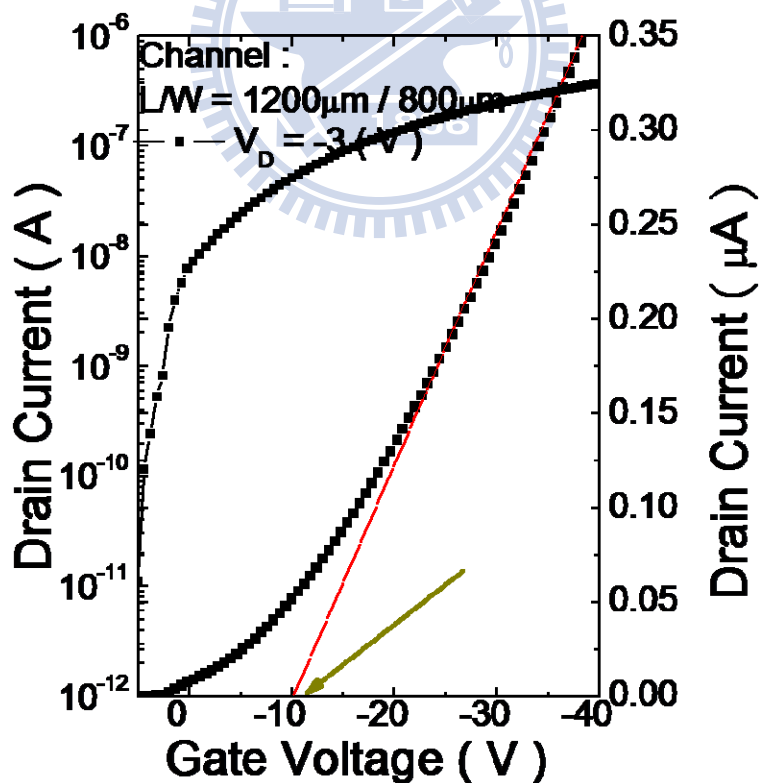


Figure 3-9. Transfer characteristics of UV-treated PMMA OTFTs

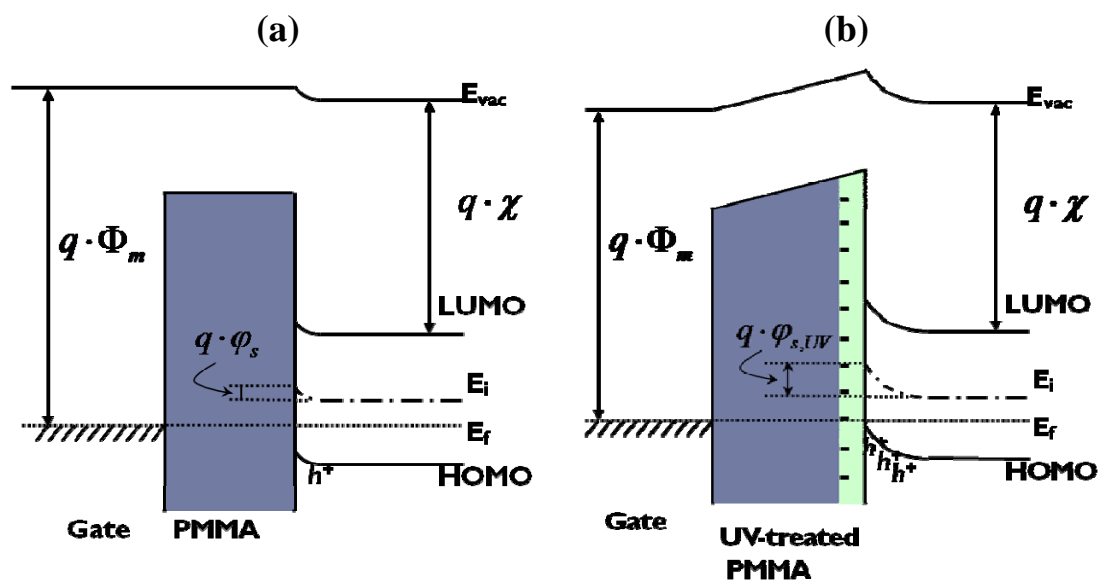
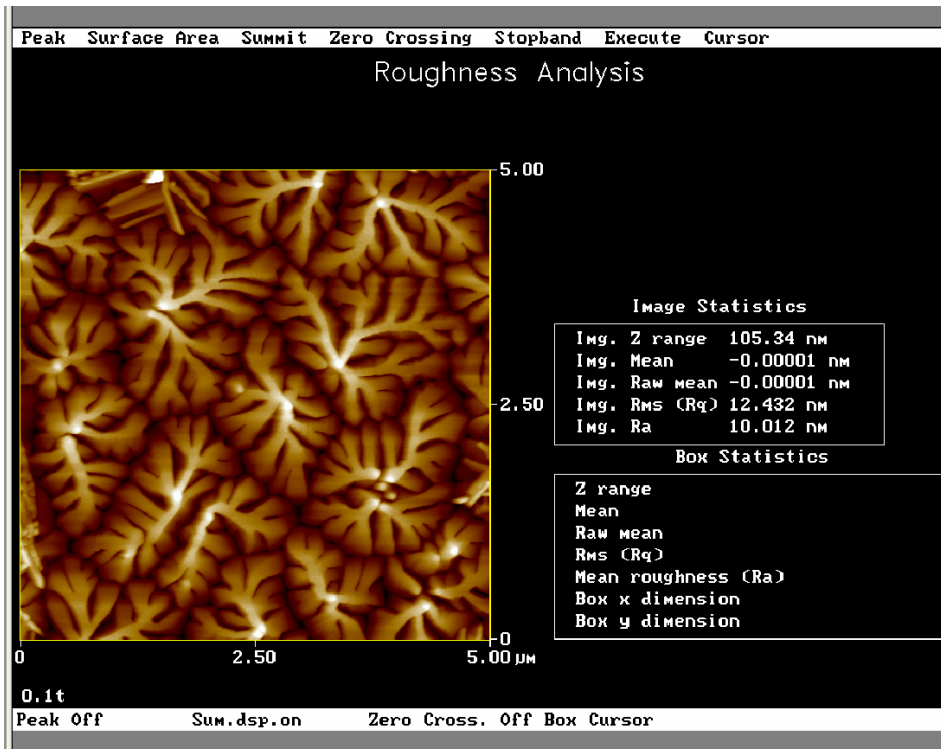


Figure 3-10. Energy band of (a) standard OTFTs and (b) UV-treated PMMA OTFTs



(a)



(b)

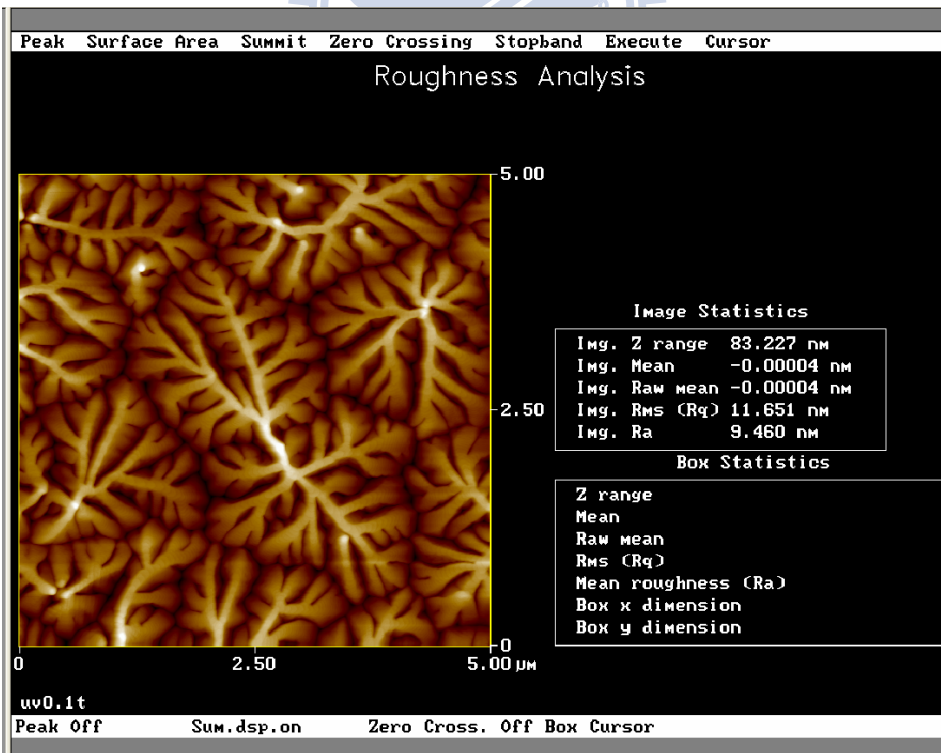
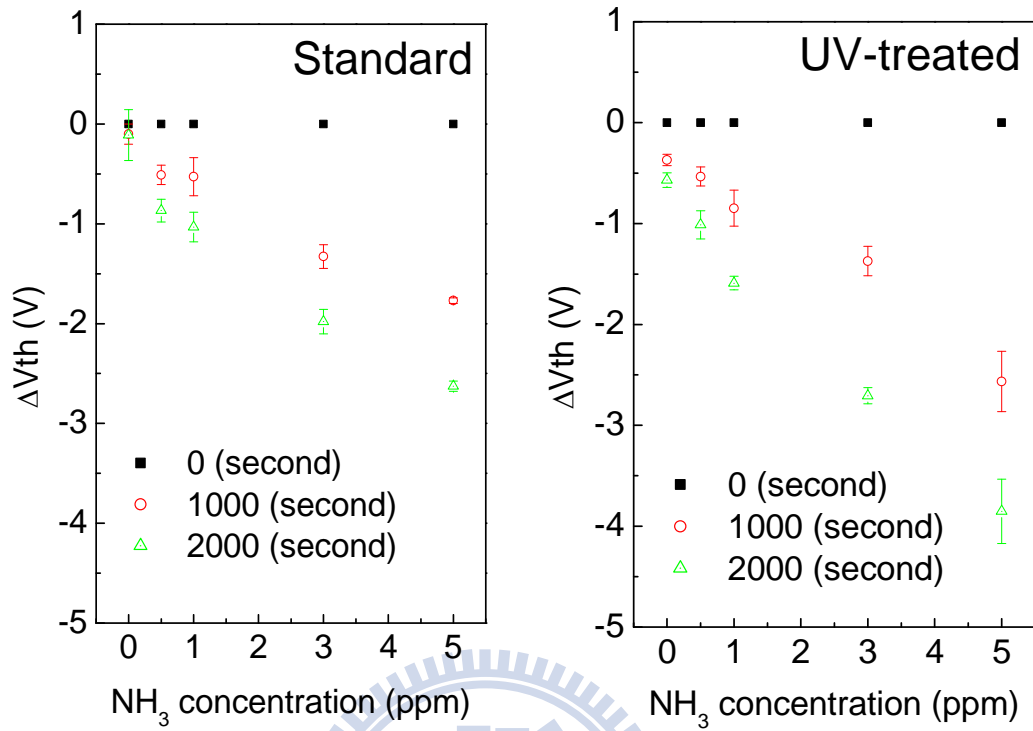
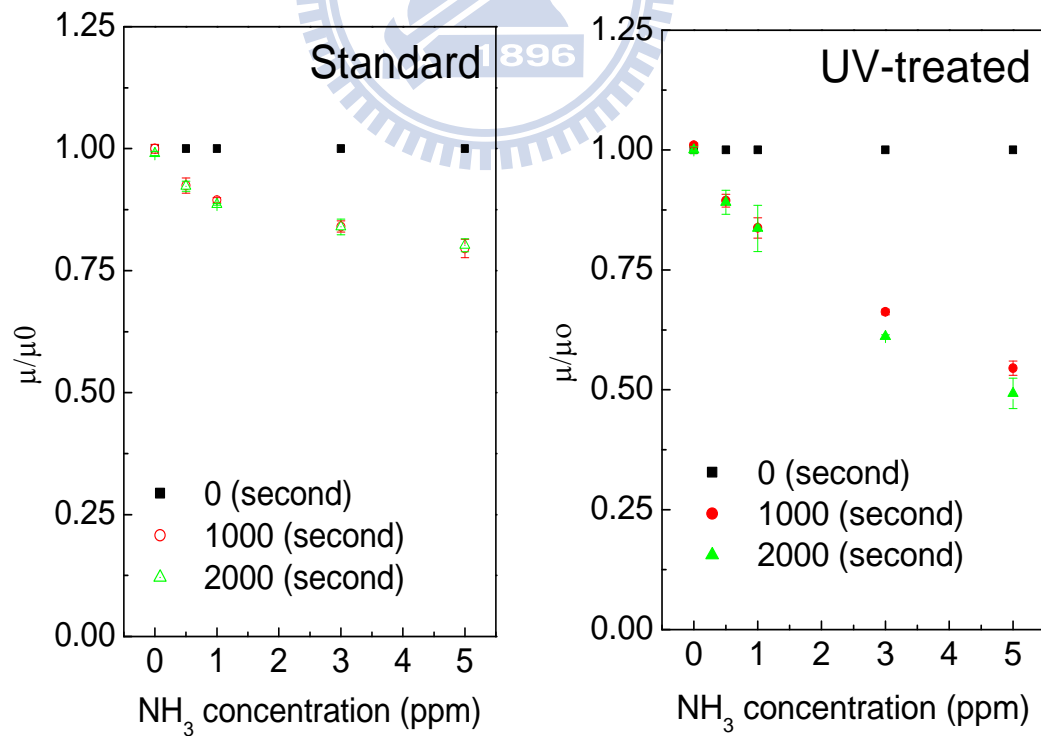


Figure 3-11. AFM images of pentacene film deposited on
(a) PMMA and (b) UV-treated PMMA

(a)



(b)



(c)

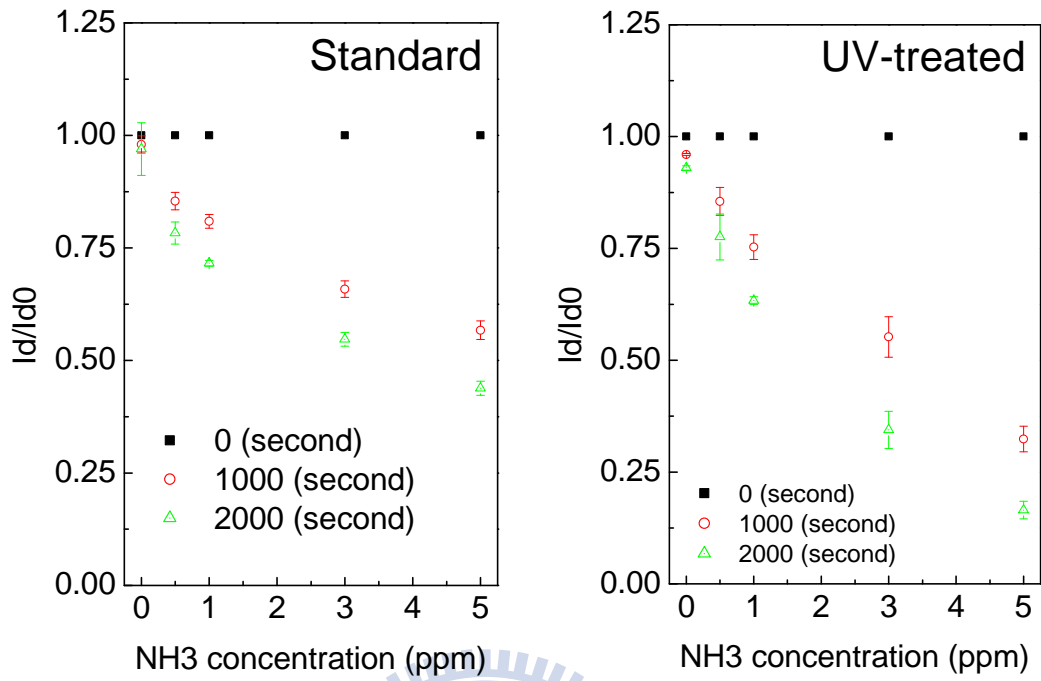


Figure 3-12. (a) Threshold voltage shift (ΔV_{th}) (b) mobility variation (μ/μ_0) and (c) drain current variation (I/I_0) versus ammonia concentration in different waiting time of standard OTFTs and UV-treated PMMA OTFTs

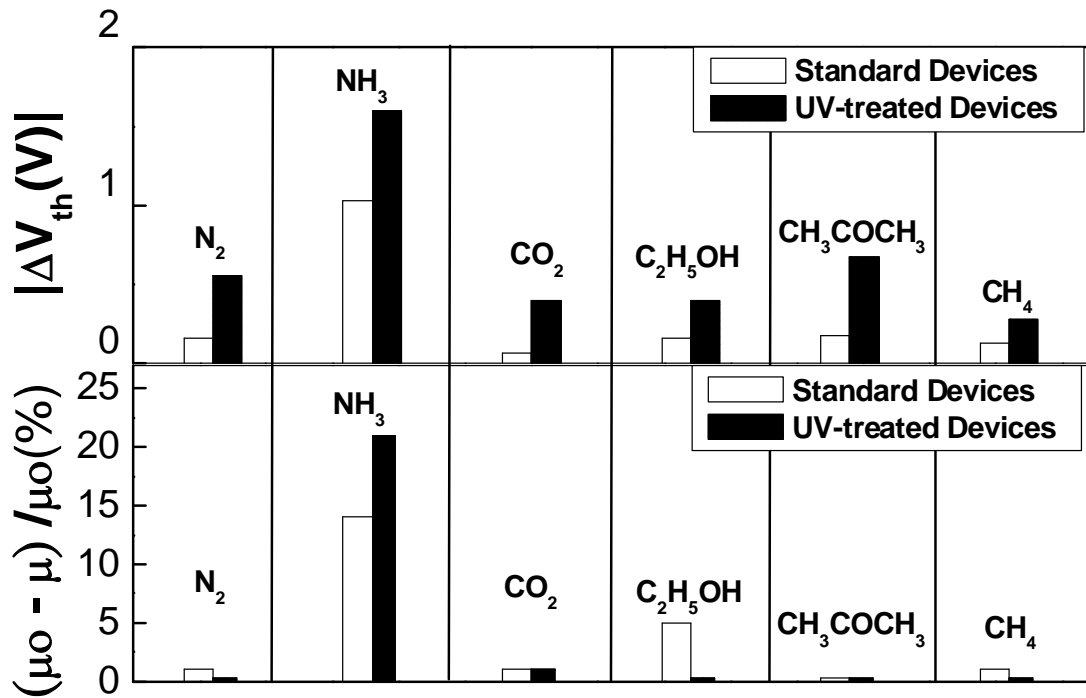


Figure 3-13. Threshold voltage shift (ΔV_{th}) and mobility variation $((\mu_0 - \mu) / \mu_0)$ percentage for standard and UV-treated OTFTs when devices were exposed to different kinds of gas molecules.

(a)

(b)

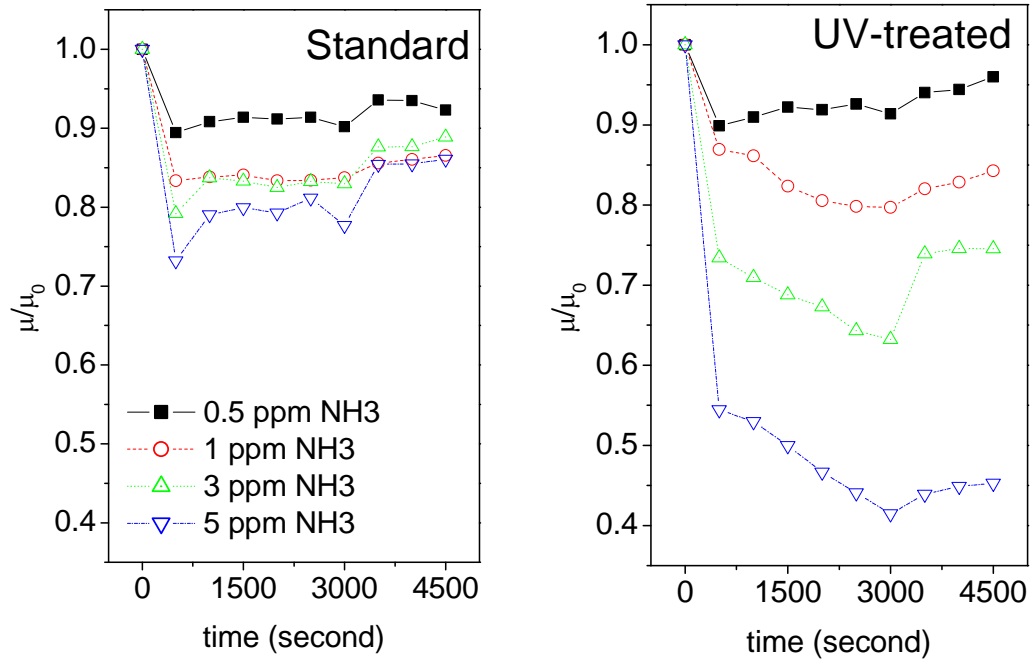


Figure 3-14. Mobility variation versus different time of (a) standard OTFTs and (b) UV-treated PMMA OTFTs under different ammonia concentration from 0 second to 3000 seconds

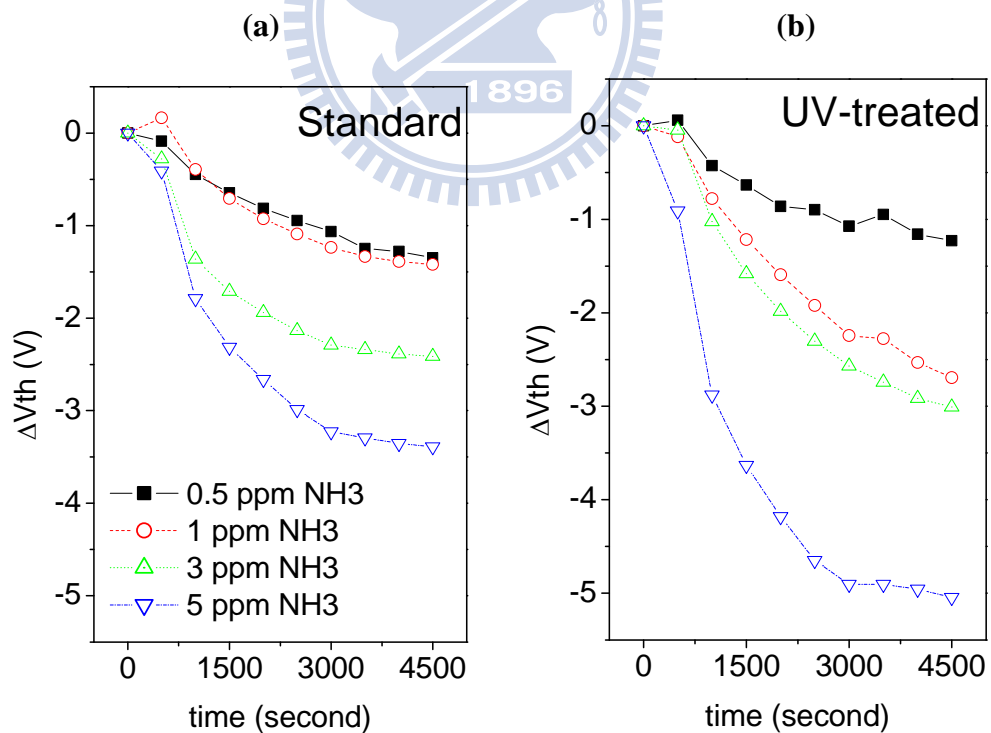


Figure 3-15. Threshold voltage shift versus different time of (a) standard OTFTs and (b) UV-treated PMMA OTFTs under different ammonia concentration

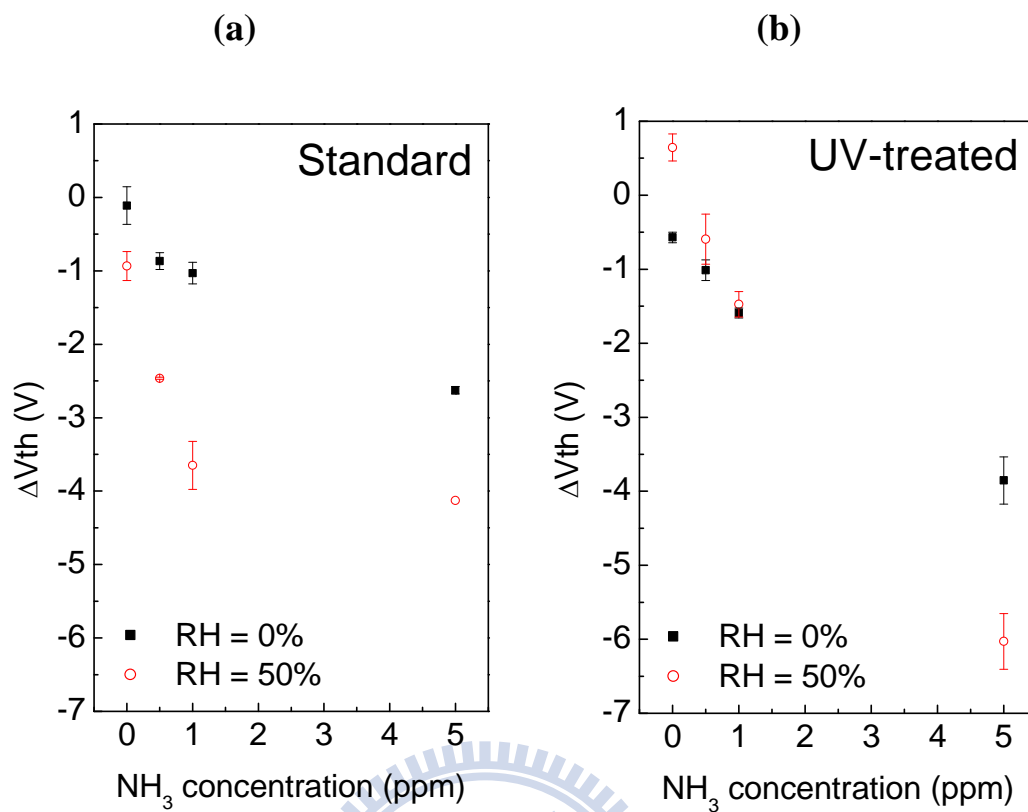


Figure 3-16. Threshold voltage shift versus different NH₃ concentrations in the dry ambient (RH=0%) and in the wet ambient (RH=50%) of **(a)** standard OTFTs and **(b)** UV-treated PMMA OTFTs

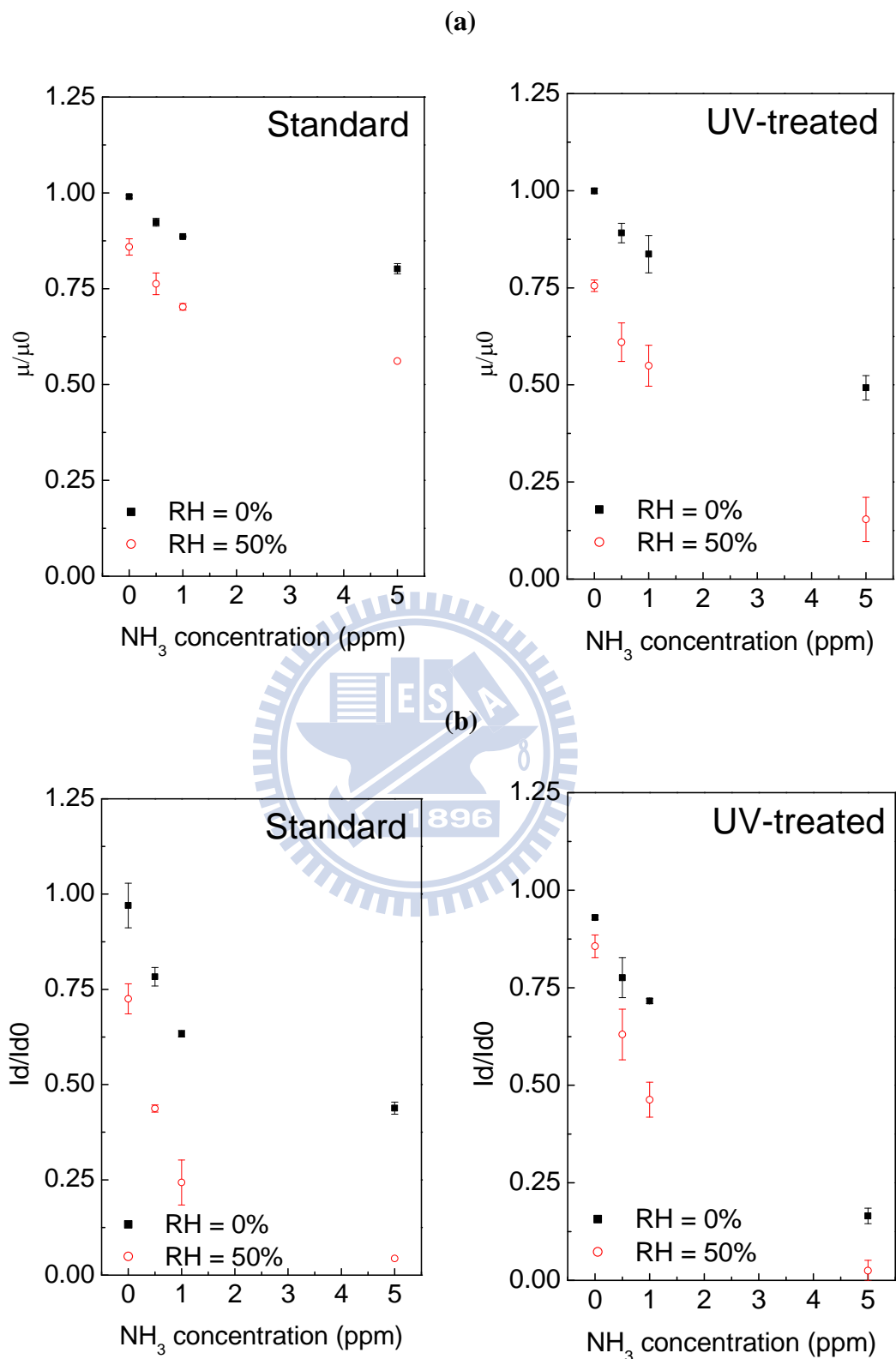


Figure 3-17. (a) Mobility variation and (b) drain current variation versus different NH₃ concentrations in the dry ambient (RH=0%) and in the wet ambient (RH=50%) of standard OTFTs or UV-treated PMMA OTFTs

Chapter 4

Conclusion

A pentacene-based OTFT was shown to be highly sensitive for ammonia sensing from 0.5 to 5 ppm, a critical range for the diagnosis of patients with chronic liver diseases and renal failure. This demonstrated that OTFT devices, which can be fabricated by simple and cheap process and exhibited channel length and width as large as several hundreds of microns, are useful as non-invasive biomedical sensors. This is on the contrary to inorganic MOSFET devices that require high fabrication cost and complicated fabrication process to scale down its dimension to the range of nanometers to increase the gas sensing sensitivity. The sensitivity and selectivity of OTFTs as gas sensor can be further improved by the modification of the PMMA dielectric layer, selecting suitable measuring parameters and providing additional local electric field. Due to the simple fabrication processes of the devices, OTFTs are promising to be developed to a portable and disposable gas sensor.

Reference

- [1] Y. Y. Lin, D. J. Gundlach, S. F. Nelson, and T. N. Jackson, IEEE Trans. Electron Devices 44, 1325 (1997)
- [2] G. Horowitz, M. E. Hajlaoui, and R. Hajlaoui, J. Appl. Phys. 87, 4456 (2000)
- [3] D. Knipp, R. A. Street, A. Volkel, and J. Ho, J. Appl. Phys. 93, 347 (2003)
- [4] A. Volkel, R. A. Street, and D. Knipp, Phys. Rev. B 66, 195336 (2002)
- [5] G. Horowitz, Adv. Mater. (Weinheim, Ger.) 10, 365 (1998)
- [6] H. E. Katz and Z. Bao, J. Phys. Chem. B 104, 671 (2000)
- [7] C. D. Dimitrakopoulos, S. Purushothanman, J. Kymissis, A. Callegari, and J. M. Shaw, Science 283, 822 (1999)
- [8] I. Manunza, A. Sulis, and A. Bonfiglio, Appl. Phys. Lett. 89, 143502 (2006)
- [9] K. Nomoto, N. Hirai, N. Yoneya, N. Kawashima, M. Noda, M. Wada, and J. Kasahara, IEEE trans. Electron Devices 52, 1519 (2005)
- [10] R. Rotzoll, S. Mohapatra, V. Olariu, R. Wenz, M. Grigas, K. Dimmler, O. Shchekin, and A. Dodabalapur, Appl. Phys. Lett. 88, 123502 (2006)
- [11] Y. H. Noh, S. Y. Park, S.-M. Seo, and H. H. Lee, Org. Electron, 7, 271 (2006)
- [12] D. K. Hwang, J. H. Park, J. Lee, J.-M. Choi, J. H. Kim, E. Kim, and S. Im, J. Electrochem. Soc. 153, G23 (2006)

- [13] C. R. Kagan, A. Afzali, and T. O. Graham, *Appl. Phys. Lett.* 86, 193505 (2005)
- [14] W. J. Kim, W. H. Koo, S. J. Jo, C. S. Kim, H. K. Baik, D. K. Hwang, K. Lee, J. H. Kim, and S. Im, *Electrochem. Solid-state Lett.* 9, G251 (2006)
- [15] A. Kahn, N. Koch, W. Gao, *J. Polym. Sci. B, Polym. Phys.* 41, 2529-2548 (2003)
- [16] G. S. Trivikrama Rao, and D. Tarakarama Rao, *Sens. Actuators B* 55, 166-169 (1999)
- [17] A. Karthigeyan, R. P. Gupta, K. Scharnagl, M. Burgmair, S. K. Sharma, I. Eisele, *Sens. Actuators B* 85, 145-153 (2002)
- [18] D. Mutschall, K. Holzner, E. Obermeier, *Sens. Actuators B* 36, 320-324 (1996)
- [19] K. P. Kakde, D. J. Shirale, H. J. Kharat, P. D. Gaikwad, P. A. Savale, V. K. Gade, M. D. Shirsat, *Proceedings of NSPTS-11, C 17-1-5* (2006)
- [20] A. L. Kukla, Y. M. Shirshov, S. A. Piletsky, *Sens. Actuators B* 37, 135-140 (1996)
- [21] V. V. Chabukswar, S. Pethkar, A. A. Athawale, *Sens. Actuators B* 77, 657-663 (2001)
- [22] G. Lahdesmaki, A. Lewenstam, A. Ivaska, *Talanta* 43, 125-134 (1996)
- [23] X. Wang, N. Miura, N. Yamazoe, *Sens. Actuators B* 66, 74-76 (2000)
- [24] C. N. Xu, N. Miura, Y. Ishida, K. Matuda, N. Yamazoe, *Sens. Actuators B* 65, 163-165 (2000)
- [25] Y. Wang, X. Wu, Q. Su, Y. Lee, Z. Zhou, *Solid-state Electron.* 45, 347-350 (2001)

- [26] F. Winqvist, A. Spetz, I. Lundstrom, *Anal. Chim. Acta* 164, 127-138 (1984)
- [27] I. Lundstrom, A. Spetz, F. Winqvist, U. Ackelid, H. Sundgren, *Sens. Actuators B* 1 (1-6),15-20 (1990)
- [28] E. Palmqvist, C. Berggren Kriz, K. Svanberg, M. Khayyami, D. Kriz, *Biosens. Bioelectron.* 10, 283-287 (1995)
- [29] I. Lahdesmaki, A. Lewenstam, A. Ivaska, *Talanta* 43, 125-134 (1996)
- [30] M. P. E. Berthelot, *Repertoire Chimique Appliquee* 284 (1859)
- [31] P. L. Saerle, *Analyst* 109, 549-568 (1984)
- [32] G. H. Mount, B. Rumberg, J. Havig, B. Lamb, H. Westberg, D. Yonge, K. Johson, R. Kincaid, *Atmos. Environ.* 36 (11), 1799-1810 (2002)
- [33] B. Crone, A. Dodabalapur, A. Gelperin, L. Torsi, H. E. Katz, A. J. Lovinger, Z. Bao, *Appl. Phys. Lett.* 78, 2229-2231 (2001)
- [34] M. C. Tanese, L. Torsi, N. Cioffi, D. Colangiuli, G. M. Farinola, F. Babudri, F. Naso, M. M. Giangregorio, L. A. Zotti, L. Sabbatini, P. G. Zambonin, *Sens. Actuators B* 100, 17-21 (2004)
- [35] D. Fine, D. Cauble, T. Jung, H. von Seggern, M. Krische, A. Dodabalapur, *APS Meeting* (2003)
- [36] T. Someya, H. E. Katz, A. Gelperin, A. J. Lovinger, A. Dodabalapur, *Appl. Phys. Lett.* 81, 3079-3081 (2002)

- [37] L. Torsi, M. C. Tanese, N. Cioffi, M. C. Gallazzi, L. Sabbatini, P. G. Zambonin, G. Raos, S. V. Meille, M. M. Giangregorio, *J. Phys. Chem. B* 107, 7589-7594 (2003)
- [38] Z. -T. Zhu, J. T. Mason, R. Dieckermann, G. Malliaras, *Appl. Phys. Lett.* 81, 4643-4645 (2002)
- [39] T. Someya, T. Sekitani, S. Iba, Y. Kato, H. Kawaguchi, T. Sakurai, *Proc. Natl. Sci. USA* 101, 9966-9970 (2004)
- [40] L. Torsi, A. Dodabalapur, L. Sabbatini, P. G. Zambonin, *Sens. Actuators B* 67, 312-316 (2000)
- [41] L. Torsi, A. J. Lovinger, B. Crone, T. Someya, A. Dodabalapur, H. E. Katz, A. Gelperin, *J. Phys. Chem. B* 106, 12.563-12.568 (2002)
- [42] L. Wang, D. Fine, A. Dodabalapur, *Appl. Phys. Lett.* 85 (26), 6386-6388 (2004)
- [43] M. J. Powell, *Appl. Phys. Lett.* 43, 597-599 (1983)
- [44] H. L. Cheng, Y. S. Mai, W. Y. Chou, and L. R. Chang, *Appl. Phys. Lett.* 90, 171926 (2007)
- [45] C. D. Dimitrakopoulos, A. R. Brown, A. Pomp, *J. Appl. Phys.* 80, 2501 (1996).
- [46] L. Takeya, T. Nishikawa, T. Takenobu, S. Kobayashi, Y. Iwaea, T. Mitani, *Appl. Phys. Lett.* 85, 5078 (2004)
- [47] D. J. Gundlach, T. N. Jackson, D. G. Schlom, and S. F. Nelson, *Appl. Phys. Lett.* 74, 3302 (1999).

- [48] S. V. Novikov, D. H. Dunlap, V. M. Kenkre, P. E. Parris, and A. V. Vannikov, *Phys. Rev. Lett.* 81, 4472 (1998)
- [49] K. P. Pernstich, S. Haas, D. Oberhoff, C. Goldmann, D. J. Gundlach, B. Batlogg, A. N. Rashid, and G. Schitter, *J. Appl. Phys.* 96, 11 (2004)
- [50] C. Shimamoto, I. Hirata, and K. Katsu, *Hepato-Gastroenteral*, 47, 443 (2000)
- [51] A. Manolis, *Clin. Chem.* 29, 5 (1983)
- [52] H. W. Zan and K. H. Yen, *Electrochem. Solid-state Lett.* 118 H222-H225 (2008)
- [53] A. Bolognesi, M. Berliocchi, M. Manenti, A. D. Carlo, P. Lugli, K. Lmimouni, C. Dufour, *IEEE Trans. Electron Device* 51, 1997 (2004)
- [54] S. Scheinert, G. Paasch, M. Schrodner, H. -K. Roth, S. Sensfuss, Th. Doll, J. Appl. Phys. 92, 330 (2002)
- [55] K. P. Pernstich, S. Haas, D. Oberhoff, C. Goldmann, D. J. Gundlach, B. Batlogg, A. N. Rashid, G. Schitter, *J. Appl. Phys.* 96, 6431 (2004)
- [56] J. Takeya, T. Nishikawa, T. Takenobu, S. Kobayashi, Y. Iwasa, T. Mitani, C. Goldmann, C. Krellner, B. Batlogg, *Appl. Phys. Lett.* 85, 5078 (2004)
- [57] Y. S. Yang, S. H. Kim, S. C. Lim, J. -I. Lee, J. H. Lee, L. -M. Do, T. Zyung, *Appl. Phys. Lett.* 83, 3939 (2003)
- [58] D. Li, E. J. Borkent, R. Nortrup, H. Moon, H. Katz, and Z. Bao, *Appl. Phys. Lett.* 86, 042105 (2005)

[59] K. N. U. Narayanan, D. S. Sylvie, J. M. Nunzi, J. Phys. D: Appl. Phys. 38, 1148

(2005)

[60] S. H. Kim, H. Yang, S. Y. Yang, K. Hong, D. Choi, C. Yang, D. S. Chung, and C.

E. Park, Organic electronics 9, 673-677 (2008)

[61] D. H. Dunlap, P. E. Parris, and V. M. Kenkre, Phys. Rev. Lett. 77, 542 (1996)

[62] D. Zou and T. Tsutsui, J. Appl. Phys. 87, 1951 (2000)

